Postprint of: Mohammad Malikan, Van Bac Nguyen, Buckling analysis of piezo-magnetoelectric nanoplates in hygrothermal environment based on a novel one variable plate theory combining with higher-order nonlocal strain gradient theory, Physica E: Low-dimensional Systems and Nanostructures, Vol. 102 (2018), pp. 8-28. https://doi.org/10.1016/j.physe.2018.04.018.

Buckling analysis of piezo-magnetoelectric nanoplates in hygrothermal environment based on a novel one variable plate theory combining with higher-order nonlocal strain gradient theory

Mohammad Malikan [a *], Van Bac Nguyen [b]

[a] Department of Mechanical Engineering, Faculty of Engineering,

Islamic Azad University, Mashhad Branch, Mashhad, Iran

[b] Department of Mechanical Engineering and the Built Environment,

College of Engineering and Technology, University of Derby, Derbyshire, United Kingdom

Abstract

In the present investigation, a new first-order shear deformation theory (OVFSDT) on the basis of the in-plane stability of the piezo-magnetoelectric composite nanoplate (PMEN) has been developed, and its precision has been evaluated. The OVFSDT has many advantages compared to the conventional first-order shear deformation theory (FSDT) such as needless of shear correction factor, containing less number of unknowns than the existing FSDT and strong similarities with the classical plate theory (CPT). The composite nanoplate consisted of $BaTiO_3$-$CoFe_2O_4$, a kind of material by which coupling between piezoelectric and piezomagnetic in nanosize was established. The plate is surrounded by a motionless and stationary matrix that is embedded in a hygrothermal surround in order to keep it more stable, and to take into consideration the influences of the moisture and temperature on the plate's mechanical behavior. The governing equilibrium equations for the smart composite plate have been formulated using the higher-order nonlocal strain gradient theory within which both stress nonlocality and second strain gradient size-dependent terms are taken into account by using three independent length scale parameters. The extracted equations are solved by utilizing the analytical approaches by which numerical results are

[*] Corresponding Author: Email: Mohammad.Malikan@yahoo.com, Call No.: +98 938 778 0652

obtained with various boundary conditions. In order to evaluate the proposed theory and methods of solution, the outcomes in terms of critical buckling loads are compared with those from several available well-known references. Finally, after determining the accuracy of the results of the new plate theory, several parameters are investigated to show the influences of material properties of the ceramic composite nanoplate on the critical buckling loads.

Keywords: New first-order shear deformation theory; Piezo-magnetoelectric composite nanoplate; Higher-order nonlocal strain gradient theory; Critical buckling load

1. Introduction

The recognition of smart composite nanoceramics in material science and engineering applications in the last few years has been one of the most important achievements by researchers all over the world. The importance of smart ceramics such as piezoelectric and magneto-electro-thermal elastic ceramics in the development of advanced precise structures in material science and engineering technologies would be clearer when noting that access to High Tech in all areas without the use of a piece of smart ceramics in its original structures has not been possible before. The existence of electrical, electronic, chemical, mechanical, and magnetic properties of these materials have made them more and more widespread tendency in a wide range of applications as they not only transformed electronics, optics, and magnetism but also significantly changed their applications, resulting in constructing the small-scale devices with self-controlling and self-monitoring capabilities.

Among the multi-ferroic composites nanoceramics, the $BaTiO_3$ including ferroelectric with large piezoelectric effects and $CoFe_2O_4$ consisting ferromagnetic with large magnetostriction showed an effective and possible magneto-electric conversion with regards to the electrically/magnetically fields which led to solid deformation [1]. They have become a single composite material with both phases including magnetic and electric fields. This kind of material is interesting due to its capability to control the magnetization (or magnetic polarization) by an electric field or a magnetic one, respectively [2-3]. The coupling influences enabled the use of a multi-ferroic composite potential in electronics chips, transducers, capacitors and electromagnetic filters [4-5]. In order to produce such a smart composite

material, the $BaTiO_3$ powder was mixed with $CoFe_2O_4$ powder and then they were sintered by common ceramic processing to create the $BaTiO_3$-$CoFe_2O_4$ [6-10].

Discussions of mechanical behavior of smart piezo-magnetoelectric composite nanoplates (PMEN) have been intensively presented in the past investigations, especially on the basis of the lower-order theories such as nonlocal elasticity theory and strain gradient theories. Ke et al. [11-12] studied the nonlinear frequencies and also post-buckling of nonlocal moderately thick piezoelectric nanobeams subjected to electro-thermo-elastic loads. Jiang and Yan [13] established the stability and vibration of a nano ferroelectric plate by considering surface influences. The vibration of a non-homogeneous shell placed in a piezoelectric substrate was reported by Fang and Zhu [14]; in this study, nonlinear strains were embedded in shell theory and a numerical procedure was deployed in the equations in order to solve the simple edge condition. Fang et al. [15] utilized the surface energy influence on nonlinear frequencies of a piezoelectric nanoshells by considering orthotropic behavior. Jamalpoor et al. [16] considered biaxial stability and vibrations of a bi-layer electro/magneto nanosystem resting on a viscoelastic foundation using Eringen's nonlocal continuum theory on the basis of Kirchhoff′s hypothesis. Gholami and Ansari [17] studied the buckling and post-buckling behaviour of a rectangular PMEN plate based on a higher-order shear deformation theory. They used Parabolic, Trigonometric, Hyperbolic and Exponential shear deformable theories with various edge conditions and the nonlocal continuum theory was used in order to consider the influences of nanoscale on the nonlinear post-buckling behaviour of thick and moderately thick rectangular PMEN subjected to the compressive in-plane loads. Arefi and Zenkour [18] investigated a PMEN plate under frequency and dynamic conditions and had a viscoelastic matrix under the nanoplate. In this study, the constitutive equations and boundary conditions were derived by classical continuum theory of plate, and Eringen's nonlocal differential term has been implemented into the equations in order to examine the impact of the nanoscale on the vibration behavior of the plate. Sahmani and Aghdam [19] presented the post-buckling and buckling of a magneto-electric composite nanoshell by combining the classical plate theory and lower-order nonlocal strain gradient model; a perturbation method was considered to solve the related

equations. Gholami et al. [20] studied thermo-electro-mechanical vibration of post-buckled piezoelectric Timoshenko nanobeams based on the nonlocal elasticity theory. The governing differential equations were discretized by using the general differential quadrature (GDQ) method and then were solved by applying Newton-Raphson technique. The most important results of this investigation showed that the dimensionless natural frequencies in the post-buckling domain related to the increase of positive voltages and the decrease of negative voltages as the magnitude of voltage gets larger, and this was contrary to those happened in pre-buckling domain. Ansari et al. [21] analyzed the size-dependent nonlinear forced vibration analysis of magneto-electro-thermo-elastic Timoshenko nanobeams based upon the nonlocal elasticity theory. Whilst Sadeghi et al. [22] employed a third-order shear deformable theory for nonlinear forced vibration of nonlocal magneto-electro-thermo elastic nanobeams. They used nonlocal elasticity theory of Eringen and applied the GDQ for discretising the governing equations. Thereafter, using a Galerkin-based numerical technique, a set of nonlinear governing equations was reduced into a time varying set of ordinary differential equations of the Duffing type. The most important outcomes were presented that the natural frequency of nanobeams increased, whereas the amplitude peak decreased when the initial external magnetic potential became larger. Ansari and Gholami [23] considered a nonlocal nonlinear first-order shear deformable beam model for the post-buckling analysis of magneto-electro-thermo-elastic (METE) nanobeams. A numerical solution procedure based on the GDQ was utilized and the Eringen's nonlocal elasticity theory was applied. The results revealed that the critical buckling load and post-buckling load-carrying capacity of METE nanobeams decreased when there was an increase in the non-dimensional nonlocal parameter or when the temperature raised. Gholami et al. [24] presented a study on size-dependent higher-order shear deformable plate model for magneto-electro-thermo-elastic rectangular nanoplates by adopting the nonlocal elasticity theory to capture the size effect, and by utilizing a generalized shape function to consider the effects of transverse shear deformation and rotary inertia. They investigated parabolic, trigonometric, hyperbolic and exponential shear deformation plate theories. The results of simply-supported nanoplates were obtained based upon using the Navier's solution. Malikan [25] studied temperature influences on the shear stability of a piezoelectric nanoplate by applying a simple first-

order shear deformation theory for various boundary conditions. Ansari and Gholami [26] investigated a nonlocal nonlinear first-order shear deformable plate model for investigating the buckling and post-buckling of magneto-electro-thermo elastic nanoplates under magneto-electro-thermo-mechanical loadings. The nonlocal elasticity theory within the framework of the first-order shear deformation plate theory was used in conjunction with the generalized differential quadrature method. Ansari and Gholami [27] considered the small scale effect together with the influences of transverse shear deformation, rotary inertia and the magneto-electro-thermo-mechanical coupling, the linear free vibration of magneto-electro-thermo-elastic rectangular nanoplates with various edge supports in pre- and post-buckled states. The nonlinear governing equations and the corresponding boundary conditions were derived using Hamilton's principle which were then discretized via the GDQ method. In addition, Ansari and Gholami [28] studied size-dependent geometrically nonlinear free vibration of magneto-electro-thermo elastic nanoplates using the nonlocal elasticity theory. The mathematical formulation was developed based on the first-order shear deformation plate theory, von Kármán-type of kinematic nonlinearity and nonlocal elasticity theory. The GDQ method was utilized to reduce the nonlinear partial differential equations to a system of time-dependent nonlinear ordinary differential equations. Afterwards, the numerical Galerkin's method and periodic time differential operators were employed to compute the nonlinear frequency versus the amplitude for the nanoplates.

It is now clear that the lower-order nonlocal theories such as Eringen's nonlocal elasticity theory have been widely employed for studying nanoscale materials. However, the ability of nonlocal elasticity theory in determining the size-dependence of nanostructures is limited due to that the strain gradient elasticity is not included in the energy density in Eringen's formulation [29] and the fact is that it could be only possible to predict the interaction effects of atoms in a domain by using the stress gradient parameter. Unlike the nonlocal elasticity theory, the strain gradient theory enabled including the strain gradient parameter effect by utilizing an additional factor called strain gradient length scale (SGLS) parameter. On the other hand, the modified couple stress theories are forms of strain gradient theories but have been rarely used for nanoscale materials as they only included ***first strain gradient***. In fact, the

couple stress theories are weak in examining nanomaterials due to the lack of ***surface nonlocality*** in the theory [30]. Surface nonlocality could be defined with second gradient parameters due to physical explanation of Laplacian and the couple stress theories just represented the material hardness increased with decreasing material size from macro to micro [25]. Micro and nano tests have shown that the material hardness increased with decreasing size [31-33]. Generally, the classical continuum theory is not able to predict the size dependency since it does not possess an intrinsic material length-scale. As an explicit definition of Laplacian operator, the Laplacian term in size-dependent theories means that the potential energy-density value at a reference point is equal to the average energy of all the points around it. In two dimensions, the around points are considered as a circle with radius R around the reference point. Using this assumption, it can be approved that both stresses and strains are in an average form of domain for a reference point in the nonlocal strain gradient theory. The major aim for using nonlocal strain gradient theory is to synthesize both ***second stress and strain gradient parameters*** in a unique theory. This might result in stronger nonlocality.

Since the deformations of nanostructures are complex, applying continuum models with lower-order nonlocal deformation mechanism might be uncertain in order to correctly obtain the mechanical characteristics. The higher-order nonlocal strain gradient theory contained higher and lower-order nonlocal stresses and strains [34]. The higher-order nonlocal stresses are significant for analysing large deformations so there has been an urgent need to consider them. Therefore, in this research, the main motivation is to use the higher-order nonlocal strain gradient theory to differentiate between higher and lower-order stresses in some situations of the analysis.

Since the nano materials are size-dependent ones, there are some additional parameters in constitutive equations to take into account their fundamental mechanical behavior in nanoscale when continuum models are used. The higher-order nonlocal strain gradient theory used in the current research to consider a new theory for nanomaterials. There are some interior parameters which could be appeared in the mathematical presentation of the results. In light of the fact that these determinative parameters could help predict mechanical behavior of nanostructures without spending high costs on the model in

experimental's tests, so their adaptable values have to be used. However, there have never been such values available, although some researchers found close amounts [35-38]. In addition, the use of additional physical parameters in the formulation of the any theory usually leads to difficulties in determining suitable values for these parameters, e.g. SGLS parameter. This parameter showed effect of small size and could be taken values in between zero to unspecified positive micro/nano values which have to be determined in laboratory for various nanomaterials under many situations. It is known that for nanomaterials it has not been determined and there are only few materials for which the parameter is given based on experimental's testing [35-38]. Therefore, the parameter could be chosen as a non-dimensional changeable factor so that it could be applicable in the theory development [25]. Another parameter in the theory is nonlocal parameter which also defines the small size effect and depends on the crystal structure in lattice dynamics and the nature of physics of the material [39-43]. It is clear that determining values for such a parameter by either a laboratory work or in a computer simulation has many difficulties and high costs. Therefore, it could be possible by determining a good range of values for the parameter [42-43].

Most of the industrial environments are under humidity and heat conditions in which the materials or pieces of machines are confronted by critical conditions which lead to unpredictable damages. Therefore, mechanical stress induced in such conditions should be analyzed in order to take into account the impacts of moisture and temperature on the stress behavior. By placing the $BaTiO_3$-$CoFe_2O_4$ nanoceramics plate in a hygrothermal environment, it could be possible to gain more realistic outcomes [44].

In this paper, a new plate theory developed by reducing the unknown variables from a regenerated first-order shear deformation theory is presented. A ceramic composite nanoplate using $BaTiO_3$-$CoFe_2O_4$ is considered to be in a hygrothermal environment and is coupled by a polymer foundation. The nanoplate is subjected to biaxial compression, and an electric voltage and a magnetic potential are exerted on the model. Both stress and strain gradient parameters for the nano model are examined by using higher-order nonlocal strain gradient (HONSG) theory which could result in new outcomes. Furthermore,

analytic approaches are employed to solve the critical buckling equations by assuming several boundary conditions for the nanoceramics plate.

2. Formulation

2.1 One Variable First-Order Shear Deformation Theory (OVFSDT)

Fig. 1 shows an idealized and continuum PMEN presented in this article. The nanoplate is rested on the two-parameter foundation exposed to the outer in-plane mechanical load (N_0) as well as the electric voltage φ_0, and magnetic potential ψ_0 between upper and bottom surfaces in the hygrothermal surrounds. The nanoplate has the length L_x, width L_y and thickness h associated with the x, y and z-axes of the right-hand coordinate system, respectively.

Plates have been considered as important elements in engineering structures and thus have been paid significant attention by designers and researchers around the world. The extensively wide applications of the plates in several industries including aerospace, shipbuilding, reactors, constructions and other professions in recent years has required accurate approaches to analysis their mechanical behavior and begun to seriously push the boundaries of available studied methods. Heretofore, many methods have been presented for investigation of the plates. These methods included three-dimensional continuum theories and some two-dimensional procedures (the assumption that $\sigma_z=0$ has been used). Although three-dimensional elasticity analysis has confronted with complexities and difficulties, it has been so far considered as and the most realistic and precise one. The simplest theory for analysis of the plates is the classical hypothesis which is based on Kirchhoff's assumptions in which the influences of transverse shear deformation are not taken into account. In this theory, it is supposed that each planar or perpendicular sections to the mid-plane remained perpendicular on the middle surfaces during loading. This is an appropriate theory in order to study thin plates; however, due to the ignorance of the shear and transverse strains along the thickness, this theory is accompanied with errors when using it for moderately thick and thick plates. In order to reduce the error in the analysis of relatively thick plates, another theory known as shear deformation theory is introduced. In this theory, the transverse shear effects are taken into consideration. With regard to the number of sentences placed in the expansion of

the displacement field along the thickness, the order of the theory (first, second, etc.) is determined. Although the shear deformation theories in the analysis of thick plates have shown capturing the transverse shear effects and consequently reasonable results, they are still far from obtaining exact results due to the non-consideration of the effect of transverse strain. The first-order of the shear theory called Mindlin's is accompanied with a serious error (the assumption of constant value for shear stress along the thickness of plates from upper to bottom surfaces) and for that reason the shear correction parameter has been used. This means that the assumption of constant shear stress through the entire thickness is not always correct. To overcome this deficiency and maximize the accuracy for plate analysis, a new first-order shear deformation theory (S-FSDT) has been introduced. First, according to the first-order theory (FSDT), displacement field of the plate points could be defined as follows [45]:

$$\begin{Bmatrix} U(x,y,z) \\ V(x,y,z) \\ W(x,y,z) \end{Bmatrix} = \begin{Bmatrix} u(x,y)+z\phi(x,y) \\ v(x,y)+z\psi(x,y) \\ w(x,y) \end{Bmatrix} \quad \text{(1a-c)}$$

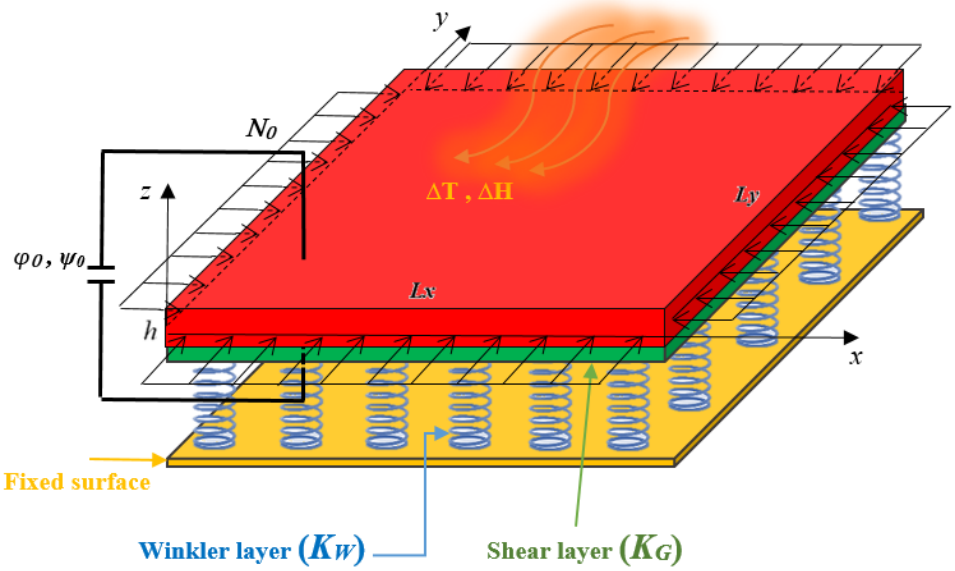

Fig. 1. Configuration of $BaTiO_3$-$CoFe_2O_4$ composite nanoceramics plate in a hygrothermal environment

In Eqs. (1), the vector quantities of the neutral axis in the directions of *x*, *y* and *z* are *u*, *v* and *w*, respectively. Furthermore, parameters ϕ and ψ are used for defining the twisting of plate's elements around *y* and *x*-axis, respectively. First of all, the S-FSDT theory is reconsidered in which it is supposed that the deflection parameter could be expressed as follows [46-50]:

$$w\left(x,y\right)=w_b\left(x,y\right)+w_s\left(x,y\right) \tag{2}$$

In which the w_b (x, y) and w_s (x, y) are the bending and shear components of deflection, respectively. On the other hand, the rotation parameters are expressed as follows:

$$\begin{Bmatrix}\phi\\ \psi\end{Bmatrix}=\begin{Bmatrix}-\dfrac{\partial w_b\left(x,y\right)}{\partial x}\\ -\dfrac{\partial w_b\left(x,y\right)}{\partial y}\end{Bmatrix} \tag{3a-b}$$

By replacing Eqs. (2-3) into Eqs. (1) the displacement field of the simple first-order shear deformation theory (S-FSDT) is rewritten [47-50]:

$$\begin{Bmatrix}U\left(x,y,z\right)\\ V\left(x,y,z\right)\\ W\left(x,y,z\right)\end{Bmatrix}=\begin{Bmatrix}u\left(x,y\right)-z\dfrac{\partial w_b\left(x,y\right)}{\partial x}\\ v\left(x,y\right)-z\dfrac{\partial w_b\left(x,y\right)}{\partial y}\\ w_b\left(x,y\right)+w_s\left(x,y\right)\end{Bmatrix} \tag{4a-c}$$

Using $w=w_b+w_s$ might not be conceptual. Therefore, the S-FSDT will be obtained based on one variable in the following:

$$\begin{Bmatrix}U\left(x,y,z\right)\\ V\left(x,y,z\right)\\ W\left(x,y,z\right)\end{Bmatrix}=\begin{Bmatrix}u\left(x,y\right)-z\dfrac{\partial w_b\left(x,y\right)}{\partial x}\\ v\left(x,y\right)-z\dfrac{\partial w_b\left(x,y\right)}{\partial y}\\ w_b\left(x,y\right)+W'\end{Bmatrix} \tag{5a-c}$$

In which W' is an indirect impact of shear deflection which would be determined.

Here, by substituting Eqs. (4) into nonlinear strains of Lagrangian, the strain field of S-FSDT is obtained as follows:

$$\begin{cases} \varepsilon_{xx} = -z\,\dfrac{\partial^2 w_b}{\partial x^2} + \dfrac{1}{2}\left(\dfrac{\partial w_b}{\partial x}\right)^2 + \dfrac{1}{2}\left(\dfrac{\partial w_s}{\partial x}\right)^2 + \dfrac{\partial w_b}{\partial x}\dfrac{\partial w_s}{\partial x} \\ \varepsilon_{yy} = -z\,\dfrac{\partial^2 w_b}{\partial y^2} + \dfrac{1}{2}\left(\dfrac{\partial w_b}{\partial y}\right)^2 + \dfrac{1}{2}\left(\dfrac{\partial w_s}{\partial y}\right)^2 + \dfrac{\partial w_b}{\partial y}\dfrac{\partial w_s}{\partial y} \\ \gamma_{yz} = \dfrac{\partial w_s}{\partial y} \\ \gamma_{xz} = \dfrac{\partial w_s}{\partial x} \\ \gamma_{xy} = -2z\,\dfrac{\partial^2 w_b}{\partial x\,\partial y} + \left(\dfrac{\partial w_b}{\partial x} + \dfrac{\partial w_s}{\partial x}\right)\left(\dfrac{\partial w_b}{\partial y} + \dfrac{\partial w_s}{\partial y}\right) \end{cases} \tag{6a-e}$$

By substituting Eqs. (6) into Hook′s law, the stress field could be calculated as follows:

$$\begin{Bmatrix} \sigma_{xx} \\ \sigma_{yy} \\ \sigma_{yz} \\ \sigma_{xz} \\ \sigma_{xy} \end{Bmatrix} = \left[Q_{ijk}\right] \begin{Bmatrix} \varepsilon_{xx} \\ \varepsilon_{yy} \\ \gamma_{yz} \\ \gamma_{xz} \\ \gamma_{xy} \end{Bmatrix} \tag{7a-e}$$

In which Q_{ijk} is the stiffness matrix for the material. After calculating Eqs. (7) from Eqs. (6) the stresses could be harvested and then by substituting Eqs. (7) into Eqs. (8) the S-FSDT stress resultants are now presented as follows:

$$\begin{bmatrix} N_{xx} \\ N_{yy} \\ N_{xy} \\ M_{xx} \\ M_{yy} \\ M_{xy} \\ Q_y \\ Q_x \end{bmatrix} = \begin{bmatrix} A_{11} & A_{12} & 0 & 0 & 0 & 0 & 0 & 0 \\ A_{21} & A_{22} & 0 & 0 & 0 & 0 & 0 & 0 \\ 0 & 0 & A_{66} & 0 & 0 & 0 & 0 & 0 \\ 0 & 0 & 0 & D_{11} & D_{12} & 0 & 0 & 0 \\ 0 & 0 & 0 & D_{21} & D_{22} & 0 & 0 & 0 \\ 0 & 0 & 0 & 0 & 0 & D_{66} & 0 & 0 \\ 0 & 0 & 0 & 0 & 0 & 0 & A_{44} & 0 \\ 0 & 0 & 0 & 0 & 0 & 0 & 0 & A_{44} \end{bmatrix} \times \int_{-h/2}^{h/2} \begin{Bmatrix} \sigma_x \\ \sigma_y \\ \sigma_{xy} \\ \sigma_x z \\ \sigma_y z \\ \sigma_{xy} z \\ \sigma_{yz} \\ \sigma_{xz} \end{Bmatrix} dz \tag{8a-h}$$

Here, the fourth equation of FSDT's governing equations [45] is adopted since it was simple to calculate w_s (based on w_b):

$$\frac{\partial M_x}{\partial x} + \frac{\partial M_{xy}}{\partial y} - Q_x = 0 \tag{9}$$

Now by substituting Eqs. (8) on the stress resultants of Eq. (9) to have:

$$D_{11}\frac{\partial^3 w_b}{\partial x^3} + \left(D_{12} + D_{66}\right)\frac{\partial^3 w_b}{\partial x\,\partial y^2} - A_{44}\frac{\partial w_s}{\partial x} = 0 \tag{10}$$

By integrating Eq. (10) with respect to *x*, simplifying and also ignoring the integral constants, the shear deflection could be obtained as follows:

$$w_s = W' = A\frac{\partial^2 w_b}{\partial x^2} + B\frac{\partial^2 w_b}{\partial y^2} \tag{11}$$

In which, terms *A* and *B* are expressed as follows:

$$A = \frac{D_{11}}{A_{44}},\quad B = \frac{D_{12} + D_{66}}{A_{44}} \tag{12a-b}$$

Afterwards, the OVFSDT can be achieved in the following equations:

$$\text{Now: } w_b = w_0 \;;\quad \begin{Bmatrix} U(x,y,z) \\ V(x,y,z) \\ W(x,y,z) \end{Bmatrix} = \begin{Bmatrix} -z\dfrac{\partial w_0(x,y)}{\partial x} \\ -z\dfrac{\partial w_0(x,y)}{\partial y} \\ w_0(x,y) + A\dfrac{\partial^2 w_0(x,y)}{\partial x^2} + B\dfrac{\partial^2 w_0(x,y)}{\partial y^2} \end{Bmatrix} \tag{13a-c}$$

By using the OVFSDT field which was mentioned in Eqs. (13), the impact of the shear deflection was embedded in the displacement field based on the bending deflection rather than using shear correction factor or w_s variant. Afterwards, by using Lagrangian strains and implementing the von Kármán strains, the OVFSDT strains field are expressed as follows:

$$\begin{cases} \varepsilon_{xx} = -z\dfrac{\partial^2 w_0}{\partial x^2} + \dfrac{1}{2}\left(A\dfrac{\partial^3 w_0}{\partial x^3} + B\dfrac{\partial^3 w_0}{\partial x\,\partial y^2} + \dfrac{\partial w_0}{\partial x}\right)^2 \\ \varepsilon_{yy} = -z\dfrac{\partial^2 w_0}{\partial y^2} + \dfrac{1}{2}\left(A\dfrac{\partial^3 w_0}{\partial x^2\partial y} + B\dfrac{\partial^3 w_0}{\partial y^3} + \dfrac{\partial w_0}{\partial y}\right)^2 \\ \gamma_{yz} = A\dfrac{\partial^3 w_0}{\partial x^2\partial y} + B\dfrac{\partial^3 w_0}{\partial y^3} \\ \gamma_{xz} = A\dfrac{\partial^3 w_0}{\partial x^3} + B\dfrac{\partial^3 w_0}{\partial x\,\partial y^2} \\ \gamma_{xy} = -2z\dfrac{\partial^2 w_0}{\partial x\,\partial y} + \left(A\dfrac{\partial^3 w_0}{\partial x^3} + B\dfrac{\partial^3 w_0}{\partial x\,\partial y^2} + \dfrac{\partial w_0}{\partial x}\right)\left(A\dfrac{\partial^3 w_0}{\partial x^2\partial y} + B\dfrac{\partial^3 w_0}{\partial y^3} + \dfrac{\partial w_0}{\partial y}\right) \end{cases} \tag{14a-e}$$

Regarding Hamilton's principle, the variation of total potential energy in whole domain of the plate (δV) is made available:

$$\delta V = \delta S + \delta\Omega = 0 \tag{15}$$

In which *S* is the strain energy and Ω is works which are done by external forces.

The potential energy of external loads could be defined as follows [25, 45]:

$$\delta\Omega = \int_0^{L_y}\int_0^{L_x}\left(k_G\nabla^2 w_0 - k_w w_0\right)\delta w_0 dxdy \tag{16}$$

where k_G and k_W denote shear and stiffness modules of the elastic matrix [45]. The strain energy by kronecker delta is calculated in the equation below:

$$\delta S = \iiint_v \left(\sigma_{ij}\delta\varepsilon_{ij} - D_k\delta E_k - B_k\delta H_k\right)dV = 0 \tag{17}$$

where σ_{ij}, ε_{ij}, D_k, E_k, B_k and H_k are stress tensor, strain tensor, electric displacement, electric field, magnetic displacement and magnetic field respectively, and are defined as follows [16-18, 27, 47, 51-52].

$$\sigma_{ij} = C_{ijkl}\varepsilon_{kl} - e_{kij}E_k - q_{kij}H_k - \lambda_{ij}\Delta T - \chi_{ij}\Delta H \tag{18}$$

$$D_i = e_{ikl}\varepsilon_{kl} + \kappa_{ij}E_k + d_{ij}H_k + p_i\Delta T \tag{19}$$

$$B_i = q_{ikl}\varepsilon_{kl} + d_{ij}E_k + \eta_{ij}H_k + p_i\Delta T \tag{20}$$

In which C_{ijkl}, e_{kij}, q_{kij}, κ_{ij}, d_{ij}, λ_{ij}, p_i and ΔH are elastic constant, piezoelectric constant, piezomagnetic constant, dielectric constant, electro-magnetic coupling, thermal moduli, pyroelectric constant and moisture concentration percentage, respectively. The tensors in Eqs. (18-20) are expanded in the following equations:

$$e_{kij} = \begin{bmatrix} 0 & 0 & \bar{e}_{31} \\ 0 & 0 & \bar{e}_{31} \\ \bar{e}_{15} & 0 & 0 \\ 0 & \bar{e}_{15} & 0 \\ 0 & 0 & 0 \end{bmatrix},\ e_{ikl} = e_{kij}^{\ T} = \begin{bmatrix} 0 & 0 & \bar{e}_{15} & 0 & 0 \\ 0 & 0 & 0 & \bar{e}_{15} & 0 \\ \bar{e}_{31} & \bar{e}_{31} & 0 & 0 & 0 \end{bmatrix},\ q_{kij} = \begin{bmatrix} 0 & 0 & \bar{q}_{31} \\ 0 & 0 & \bar{q}_{31} \\ \bar{q}_{15} & 0 & 0 \\ 0 & \bar{q}_{15} & 0 \\ 0 & 0 & 0 \end{bmatrix},\ q_{ikl} = q_{ikl}^{\ T} \tag{21a-d}$$

$$\kappa_{ij} = \begin{bmatrix} \bar{\kappa}_{11} & 0 & 0 \\ 0 & \bar{\kappa}_{11} & 0 \\ 0 & 0 & \bar{\kappa}_{33} \end{bmatrix},\ d_{ij} = \begin{bmatrix} \bar{d}_{11} & 0 & 0 \\ 0 & \bar{d}_{11} & 0 \\ 0 & 0 & \bar{d}_{33} \end{bmatrix},\ \eta_{ij} = \begin{bmatrix} \bar{\eta}_{11} & 0 & 0 \\ 0 & \bar{\eta}_{11} & 0 \\ 0 & 0 & \bar{\eta}_{33} \end{bmatrix} \tag{22a-c}$$

$$\begin{Bmatrix} \overline{e}_{31} \\ \overline{e}_{15} \\ \overline{\kappa}_{11} \\ \overline{\kappa}_{33} \\ \overline{q}_{31} \\ \overline{q}_{15} \\ \overline{d}_{11} \\ \overline{d}_{33} \\ \overline{\eta}_{11} \\ \overline{\eta}_{33} \end{Bmatrix} = \begin{Bmatrix} e_{31} - \dfrac{C_{13}e_{33}}{C_{33}} \\ e_{15} \\ \kappa_{11} \\ \kappa_{33} + \dfrac{e_{33}^2}{C_{33}} \\ q_{31} - \dfrac{C_{13}q_{33}}{C_{33}} \\ q_{15} \\ d_{11} \\ d_{33} + \dfrac{q_{33}e_{33}}{C_{33}} \\ \eta_{11} \\ \eta_{33} + \dfrac{q_{33}^2}{C_{33}} \end{Bmatrix} \tag{23a-j}$$

$$p_k = \begin{Bmatrix} \overline{p}_1 \\ \overline{p}_2 \\ \overline{p}_3 \end{Bmatrix}, \quad \begin{Bmatrix} \overline{p}_1 \\ \overline{p}_3 \end{Bmatrix} = \begin{Bmatrix} p_1 \\ p_3 + \dfrac{\lambda_{33}e_{33}}{C_{33}} \end{Bmatrix}, \quad \overline{\lambda}_{11} = \lambda_{11} - \frac{C_{13}\lambda_{33}}{C_{33}}, \quad \overline{\chi}_{11} = \chi_{11} + \frac{\chi_{33}e_{33}}{C_{33}} \tag{24a-c}$$

Regarding electro-magneto conditions, electric and magnetic potentials could be defined as linear functions in the following [16-18, 27, 47, 51-52].

$$\overline{\Phi}(x, y, z) = -\cos\left(\frac{\pi z}{h}\right)\Phi(x, y) + \frac{2z\varphi_0}{h} \tag{25a}$$

$$\overline{\Psi}(x, y, z) = -\cos\left(\frac{\pi z}{h}\right)\Psi(x, y) + \frac{2z\psi_0}{h} \tag{25b}$$

The magnetic and electric functions in the mid-plane of the plate are $\Psi(x,y)$ and $\Phi(x,y)$, the magnetic potential and electric voltage are ψ_0 and φ_0, respectively. Thereafter, the piezo-magnetoelectric field components could be expressed as follows:

$$E_k = \begin{Bmatrix} \overline{E}_x \\ \overline{E}_y \\ \overline{E}_z \end{Bmatrix} = \begin{Bmatrix} -\dfrac{\partial\overline{\Phi}}{\partial x} \\ -\dfrac{\partial\overline{\Phi}}{\partial y} \\ -\dfrac{\partial\overline{\Phi}}{\partial z} \end{Bmatrix} = \begin{Bmatrix} \cos\left(\dfrac{\pi z}{h}\right)\dfrac{\partial\Phi}{\partial x} \\ \cos\left(\dfrac{\pi z}{h}\right)\dfrac{\partial\Phi}{\partial y} \\ -\dfrac{\pi}{h}\sin\left(\dfrac{\pi z}{h}\right)\Phi - \dfrac{2\phi_0}{h} \end{Bmatrix} \tag{26a-c}$$

$$H_k=\begin{Bmatrix}\overline{H}_x\\ \overline{H}_y\\ \overline{H}_z\end{Bmatrix}=\begin{Bmatrix}-\dfrac{\partial\overline{\Psi}}{\partial x}\\ -\dfrac{\partial\overline{\Psi}}{\partial y}\\ -\dfrac{\partial\overline{\Psi}}{\partial z}\end{Bmatrix}=\begin{Bmatrix}\cos\left(\dfrac{\pi z}{h}\right)\dfrac{\partial\Psi}{\partial x}\\ \cos\left(\dfrac{\pi z}{h}\right)\dfrac{\partial\Psi}{\partial y}\\ -\dfrac{\pi}{h}\sin\left(\dfrac{\pi z}{h}\right)\Psi-\dfrac{2\psi_0}{h}\end{Bmatrix} \tag{27a-c}$$

Applying the variational formulation (δV=0) the nonlinear governing equations are derived as follows:

$$\delta w_0=0\ ;$$

$$-\frac{\partial^2 M_x}{\partial x^2}-\frac{\partial^2 M_y}{\partial y^2}-2\frac{\partial^2 M_{xy}}{\partial x\,\partial y}+A\frac{\partial^3 Q_x}{\partial x^3}+B\frac{\partial^3 Q_x}{\partial x\,\partial y^2}+A\frac{\partial^3 Q_y}{\partial x^2\partial y}+B\frac{\partial^3 Q_y}{\partial y^3}+$$

$$N_x\left(A^2\frac{\partial^6 w_0}{\partial x^6}+B^2\frac{\partial^6 w_0}{\partial x^2\partial y^4}+\frac{\partial^2 w_0}{\partial x^2}+2AB\frac{\partial^6 w_0}{\partial x^4\partial y^2}+2A\frac{\partial^4 w_0}{\partial x^4}+2B\frac{\partial^4 w_0}{\partial x^2\partial y^2}\right)+$$

$$N_y\left(A^2\frac{\partial^6 w_0}{\partial x^4\partial y^2}+B^2\frac{\partial^6 w_0}{\partial y^6}+\frac{\partial^2 w_0}{\partial y^2}+2AB\frac{\partial^6 w_0}{\partial x^2\partial y^4}+2A\frac{\partial^4 w_0}{\partial x^2\partial y^2}+2B\frac{\partial^4 w_0}{\partial y^4}\right)+$$

$$N_{xy}\left(2A^2\frac{\partial^6 w_0}{\partial x^5\partial y}+4AB\frac{\partial^6 w_0}{\partial x^3\partial y^3}+4A\frac{\partial^4 w_0}{\partial x^3\partial y}+2B^2\frac{\partial^6 w_0}{\partial x\,\partial y^5}+4B\frac{\partial^4 w_0}{\partial x\,\partial y^3}+2\frac{\partial^2 w_0}{\partial x\,\partial y}\right)+$$

$$k_G\nabla^2 w_0-k_w w_0=0$$

$$\delta\Phi=0\ ;\ \int_{-h/2}^{h/2}\left[\frac{\partial\overline{D}_x}{\partial x}cos\left(\frac{\pi z}{h}\right)+\frac{\partial\overline{D}_y}{\partial y}cos\left(\frac{\pi z}{h}\right)+\frac{\pi}{h}\overline{D}_z\,sin\left(\frac{\pi z}{h}\right)\right]dz=0$$

$$\delta\Psi=0\ ;\ \int_{-h/2}^{h/2}\left[\frac{\partial\overline{B}_x}{\partial x}cos\left(\frac{\pi z}{h}\right)+\frac{\partial\overline{B}_y}{\partial y}cos\left(\frac{\pi z}{h}\right)+\frac{\pi}{h}\overline{B}_z\,sin\left(\frac{\pi z}{h}\right)\right]dz=0 \tag{28a-c}$$

In which N_i, M_i, and Q_i *(i= x, y, xy)* are nonlocal stress resultants, respectively [45]. Then, the electric and magnetic displacements are defined in the equations below [16-18, 27, 47, 51-52]:

$$\begin{Bmatrix}\overline{D}_x\\ \overline{D}_y\\ \overline{D}_z\end{Bmatrix}=\int_{-h/2}^{h/2}\begin{Bmatrix}D_x\cos\left(\dfrac{\pi z}{h}\right)\\ D_y\cos\left(\dfrac{\pi z}{h}\right)\\ D_z\dfrac{\pi}{h}\sin\left(\dfrac{\pi z}{h}\right)\end{Bmatrix}dz=\begin{Bmatrix}E_{15}\left(A\dfrac{\partial^3 w_0}{\partial x^3}+B\dfrac{\partial^3 w_0}{\partial x\,\partial y^2}\right)+X_{11}\dfrac{\partial\Phi}{\partial x}+Y_{11}\dfrac{\partial\Psi}{\partial x}\\ E_{15}\left(A\dfrac{\partial^3 w_0}{\partial x^2\partial y}+B\dfrac{\partial^3 w_0}{\partial y^3}\right)+X_{11}\dfrac{\partial\Phi}{\partial y}+Y_{11}\dfrac{\partial\Psi}{\partial y}\\ -E_{31}\dfrac{\partial^2 w_0}{\partial x^2}-E_{31}\dfrac{\partial^2 w_0}{\partial y^2}-X_{33}\Phi-Y_{33}\Psi\end{Bmatrix} \tag{29a-c}$$

$$\begin{Bmatrix}\overline{B}_x\\ \overline{B}_y\\ \overline{B}_z\end{Bmatrix}=\int_{-h/2}^{h/2}\begin{Bmatrix}B_x\cos\left(\frac{\pi z}{h}\right)\\ B_y\cos\left(\frac{\pi z}{h}\right)\\ B_z\frac{\pi}{h}\sin\left(\frac{\pi z}{h}\right)\end{Bmatrix}dz=\begin{Bmatrix}F_{15}\left(A\frac{\partial^3 w_0}{\partial x^3}+B\frac{\partial^3 w_0}{\partial x\partial y^2}\right)+Y_{11}\frac{\partial\Phi}{\partial x}+Y_{22}\frac{\partial\Psi}{\partial x}\\ F_{15}\left(A\frac{\partial^3 w_0}{\partial x^2\partial y}+B\frac{\partial^3 w_0}{\partial y^3}\right)+Y_{11}\frac{\partial\Phi}{\partial y}+Y_{22}\frac{\partial\Psi}{\partial x}\\ -F_{31}\frac{\partial^2 w_0}{\partial x^2}-F_{31}\frac{\partial^2 w_0}{\partial y^2}-Y_{33}\Phi-Y_{44}\Psi\end{Bmatrix} \tag{30a-c}$$

The coefficients in Eqs. (29-30) could be expressed as follows [16-18, 27, 47, 51-52].

$$\begin{Bmatrix}E_{31}\\ E_{15}\\ X_{11}\\ X_{33}\end{Bmatrix}=\int_{-h/2}^{h/2}\begin{Bmatrix}\overline{e}_{31}\frac{\pi}{h}z\sin\left(\frac{\pi}{h}z\right)\\ \overline{e}_{15}\cos\left(\frac{\pi}{h}z\right)\\ \overline{\kappa}_{11}\cos^2\left(\frac{\pi}{h}z\right)\\ \overline{\kappa}_{33}\left(\frac{\pi}{h}\right)^2\sin^2\left(\frac{\pi}{h}z\right)\end{Bmatrix}dz \tag{31a-d}$$

$$\begin{Bmatrix}Y_{11}\\ Y_{33}\end{Bmatrix}=\int_{-h/2}^{h/2}\begin{Bmatrix}\overline{d}_{11}\cos^2\left(\frac{\pi}{h}z\right)\\ \overline{d}_{33}\left(\frac{\pi}{h}\right)^2\sin^2\left(\frac{\pi}{h}z\right)\end{Bmatrix}dz \tag{32a-b}$$

$$\begin{Bmatrix}F_{31}\\ F_{15}\\ Y_{22}\\ Y_{44}\end{Bmatrix}=\int_{-h/2}^{h/2}\begin{Bmatrix}\overline{q}_{31}\frac{\pi}{h}z\sin\left(\frac{\pi}{h}z\right)\\ \overline{q}_{15}\cos\left(\frac{\pi}{h}z\right)\\ \overline{\eta}_{11}\cos^2\left(\frac{\pi}{h}z\right)\\ \overline{\eta}_{33}\left(\frac{\pi}{h}\right)^2\sin^2\left(\frac{\pi}{h}z\right)\end{Bmatrix}dz \tag{33a-d}$$

The tensioning and flexural stiffness matrixes of the PMEN are expressed as follows:

$$A_{ij}=\int_{-\frac{h}{2}}^{\frac{h}{2}}\overline{C}_{ij}\,dz\quad(i,j=1,2,4,6),\ D_{ij}=\int_{-\frac{h}{2}}^{\frac{h}{2}}\overline{C}_{ij}z^2\,dz\quad(i,j=1,2,6) \tag{34a-b}$$

$$\begin{Bmatrix}\overline{C}_{11}\\ \overline{C}_{12}\\ \overline{C}_{44}\\ \overline{C}_{66}\end{Bmatrix}=\begin{Bmatrix}C_{11}-\frac{C_{13}^2}{C_{33}}\\ C_{12}-\frac{C_{13}^2}{C_{33}}\\ C_{44}\\ C_{66}\end{Bmatrix} \tag{35a-d}$$

Here, the in-plane loads in pre-buckling conditions are described in the following equation:

$$N^{0} = \left[N_{ij}\right]^{Mech} + \left[N_{ij}\right]^{E} + \left[N_{ij}\right]^{Mag} + \left[N_{ij}\right]^{T} + \left[N_{ij}\right]^{H} \tag{36}$$

where $N_{ij}^{Mech}, N_{ij}^{E}, N_{ij}^{Mag}, N_{ij}^{T}$, and N_{ij}^{H} are the in-plane mechanical, electric, magnetic, thermal and hygral loads which are expressed in the following equations below [16, 44, 47, 51]:

$$N_{x}^{Mech}, N_{y}^{Mech} = -N \tag{37a}$$

$$N_{x}^{E}, N_{y}^{E} = \int_{-h/2}^{h/2} -e_{31} \frac{2\varphi_0}{h} dz \tag{37b}$$

$$N_{x}^{Mag}, N_{y}^{Mag} = \int_{-h/2}^{h/2} -q_{31} \frac{2\psi_0}{h} dz \tag{37c}$$

$$N_{x}^{T}, N_{y}^{T} = -\bar{\lambda}_{11} \int_{-h/2}^{h/2} \Delta T dz \tag{37d}$$

$$N_{x}^{H}, N_{y}^{H} = -\bar{\chi}_{11} \int_{-h/2}^{h/2} \Delta H dz \tag{37e}$$

2.2 Higher-Order Nonlocal Strain Gradient Elasticity Theory (HONSG)

It is clear that the length scales in Eringen's nonlocal elasticity theory and the strain gradient theories (strain gradient and couple stress theories) represent two entirely different physical characteristics of materials at nanoscale. Therefore, there has been a serious need to apply both of the length scales into ***a single theory*** so that the true effect of the two length scales on the structural response could be assessed [53-55]. Nonlocal strain gradient theory opened a way to develop such a size-dependent theory for investigating the nanoplate's behavior. According to this non-classical hypothesis the ***stress-gradient*** and ***strain-gradient*** parameters could be used together. In fact, by considering both second stress and strain gradient parameters there could be a strong nonlocality investigation for nanostructures.

In the present paper, the higher-order size-dependent theory is considered in order to reveal the significance of higher-order length scale parameter in the aspect of the following equations [53-55]:

$$\left[1-\mu_1^2\nabla\nabla\right]\left[1-\mu_0^2\nabla\nabla\right]\sigma_{ij} = C_{ijkl}\left[1-\mu_1^2\nabla\nabla\right]\varepsilon_{kl} - C_{ijkl}\, l^2\left[1-\mu_0^2\nabla\nabla\right]\nabla\nabla\varepsilon_{kl} \tag{38a}$$

$$\mu_0(nm) = e_0 a,\ \mu_1(nm) = e_1 a,\ \nabla\nabla = \frac{\partial^2}{\partial x^2} + \frac{\partial^2}{\partial y^2} \tag{38b}$$

where μ_0, μ_1, and l are lower and higher-order stress nonlocality factors and SGLS parameter, respectively. e_0 and e_1 are nonlocal elasticity constants associated with the kinds of materials [45]. Also, a is an interior determined length regarding to intrinsic properties of the material such as lattice parameter, connection length of two atoms and etc. [45, 53-55]. As a matter of fact, these ***three small scale parameters*** are ***independent*** changeable factors for small scale effects which define the dependence of mechanical responses on the structure size. And using a single separate small scale parameter in size-dependent theories (Eringen's nonlocal elasticity, couple stress and pure strain gradient theories) could not appropriately predict the wide range of small-scale phenomena behavior [56-57]. Therefore, a size-dependent theory with multiple length-scale parameters was necessary to capture the size effects of mechanical, electric and magnetic behavior of structures at nanoscale [58]. These parameters are directly related to internal properties of small size materials (granular distances, lattice parameter and many other properties [39, 59]). Moreover, a fixed value for these parameters are not always realistic because different problems could require different values.

Eq. (38a) can be therefore converted into other forms of nonlocal theory:

a) Eringen's nonlocal elasticity theory (ENET) [60] (strong nonlocality considering second stress gradient parameter, that is suitable for nanostructures [59]).

$$\left\{ l = \mu_1 = 0 \rightarrow \left(1 - \mu_0^2 \nabla^2\right)\sigma_{ij} = C_{ijkl}\,\varepsilon_{kl} \right. \tag{39}$$

b) Strain gradient elasticity theory (considers the strain gradient parameter based on the first and second strain gradient parameters of Mindlin [61-62]). Noted that the couple stress theories are forms of strain gradient theories by taking the first strain gradient parameter of Mindlin [25, 47, 63]. In couple stress theory the ***cell*** of the material can be interpreted ***as a molecule*** of a polymer, a crystallite of a polycrystal or a grain of a granular material [64-67]. In this theory, the unit cell is taken to be a parallelepiped in order to represent the unit cell of a crystal lattice. The potential energy-density is assumed to be a function of the strain and the curl of the strain

instead of the strain alone [64-67]. In the first strain gradient theory of Mindlin, the first gradient of the displacement enters the potential energy-density only in the symmetric form of strains. In fact, the potential energy-density depends on the gradient of the strain in addition to the strain itself [61-62].

$$\left\{\mu_0=\mu_1=0\rightarrow\sigma_{ij}=C_{ijkl}\left(1\pm l^2\nabla^2\right)\varepsilon_{kl}\right. \tag{40}$$

It is now vivid that the nonlocal continuum mechanics has been treated with two different aproaches [68-69]; the integral nonlocality (Eq. (39)) [39-40, 59, 70] and the gradient elasticity theory (Eq. (40)) [71]. The strain gradient in Eq. (40) with negative sign was derived from the positive-definite deformation energy density, and this model of strain gradient is stable. However, the positive sign of the strain gradient term in the equation made this term destabilizing [72-73]. By consolidating Eqs. (38), the nonlocal strain gradient elasticity theory can be achieved in the equation below.

c) Nonlocal strain gradient theory (LONSG)[74]:

$$\begin{cases}\mu_0=e_0a\\ \mu_1=e_1a\end{cases}\rightarrow\mu_0=\mu_1=\mu\ \rightarrow\left(1-\mu^2\nabla^2\right)\sigma_{ij}=C_{ijkl}\left(1-l^2\nabla^2\right)\varepsilon_{kl} \tag{41}$$

By applying nonlocal strain gradient theory, the problem might have stronger nonlocality against cases *a*, *b* by having stress-gradient and strain-gradient as second gradient parameters. It was because stress and strain gradient tensors are coupled together in energy density of the nanoplate. Mathematically interpreted based on the Taylor series expansion, the strain gradient (second gradient of deformation) is reasonable to be included in energy density to characterize the size-dependent properties [58].

Here, using the HONSG theory the stress resultants could be derived as follows [55]:

$$\left(1-\mu_1^2\nabla^2\right)\left(1-\mu_0^2\nabla^2\right)\sigma_{ij}=C_{ijkl}\left(1-\mu_1^2\nabla^2\right)\varepsilon_{kl}-C_{ijkl}l^2\left(1-\mu_0^2\nabla^2\right)\nabla^2\varepsilon_{kl}-e_{kij}E_k-q_{kij}H_k-\lambda_{ij}\Delta T-\chi_{ij}\Delta H \tag{42a}$$

$$\left(1-\mu_1^2\nabla^2\right)\left(1-\mu_0^2\nabla^2\right)D_i=C_{ijkl}\left(1-\mu_1^2\nabla^2\right)\varepsilon_{kl}-C_{ijkl}l^2\left(1-\mu_0^2\nabla^2\right)\nabla^2\varepsilon_{kl}+\kappa_{ij}E_k+d_{ij}H_k+p_i\Delta T \tag{42b}$$

$$\left(1-\mu_1^2\nabla^2\right)\left(1-\mu_0^2\nabla^2\right)B_i=C_{ijkl}\left(1-\mu_1^2\nabla^2\right)\varepsilon_{kl}-C_{ijkl}l^2\left(1-\mu_0^2\nabla^2\right)\nabla^2\varepsilon_{kl}+d_{ij}E_k+\eta_{ij}H_k+p_i\Delta T \tag{42c}$$

The stress resultants in local forms are specified by the relations below [45, 75]:

$$\left(N_x,N_y,N_{xy}\right)=\int_{-h/2}^{h/2}\left(\sigma_x,\sigma_y,\sigma_{xy}\right)dz \tag{43a}$$

$$(M_x, M_y, M_{xy}) = \int_{-h/2}^{h/2} \left(\sigma_x, \sigma_y, \sigma_{xy}\right) z dz \tag{43b}$$

$$\left(Q_x, Q_y\right) = \int_{-h/2}^{h/2} \left(\sigma_{xz}, \sigma_{yz}\right) dz \tag{43c}$$

By using Eqs. (14) and Eqs. (43), the stress resultants could be obtained as follows:

$$\begin{Bmatrix} N_{xx} \\ N_{yy} \\ N_{xy} \\ M_{xx} \\ M_{yy} \\ M_{xy} \\ Q_y \\ Q_x \end{Bmatrix}^{Total} = \begin{bmatrix} A_{11} & A_{12} & 0 & 0 & 0 & 0 & 0 & 0 \\ A_{21} & A_{22} & 0 & 0 & 0 & 0 & 0 & 0 \\ 0 & 0 & A_{66} & 0 & 0 & 0 & 0 & 0 \\ 0 & 0 & 0 & D_{11} & D_{12} & 0 & 0 & 0 \\ 0 & 0 & 0 & D_{21} & D_{22} & 0 & 0 & 0 \\ 0 & 0 & 0 & 0 & 0 & D_{66} & 0 & 0 \\ 0 & 0 & 0 & 0 & 0 & 0 & A_{44} & 0 \\ 0 & 0 & 0 & 0 & 0 & 0 & 0 & A_{44} \end{bmatrix} \times \begin{bmatrix} \frac{\partial u}{\partial x} - z\frac{\partial^2 w_0}{\partial x^2} + \frac{1}{2}\left(A\frac{\partial^3 w_0}{\partial x^3} + B\frac{\partial^3 w_0}{\partial x \partial y^2} + \frac{\partial w_0}{\partial x}\right)^2 \\ \frac{\partial v}{\partial y} - z\frac{\partial^2 w_0}{\partial y^2} + \frac{1}{2}\left(A\frac{\partial^3 w_0}{\partial x^2 \partial y} + B\frac{\partial^3 w_0}{\partial y^3} + \frac{\partial w_0}{\partial y}\right)^2 \\ \left(\frac{\partial u}{\partial y} + \frac{\partial v}{\partial x}\right) - 2z\frac{\partial^2 w_0}{\partial x \partial y} + \left(A\frac{\partial^3 w_0}{\partial x^3} + B\frac{\partial^3 w_0}{\partial x \partial y^2} + \frac{\partial w_0}{\partial x}\right)\left(A\frac{\partial^3 w_0}{\partial x^2 \partial y} + B\frac{\partial^3 w_0}{\partial y^3} + \frac{\partial w_0}{\partial y}\right) \\ -\frac{\partial^2 w_0}{\partial x^2} \\ -\frac{\partial^2 w_0}{\partial y^2} \\ -\frac{\partial^2 w_0}{\partial x \partial y} \\ A\frac{\partial^3 w_0}{\partial x^2 \partial y} + B\frac{\partial^3 w_0}{\partial y^3} \\ A\frac{\partial^3 w_0}{\partial x^3} + B\frac{\partial^3 w_0}{\partial x \partial y^2} \end{bmatrix}^{Mech}$$

$$+ \begin{Bmatrix} 2\bar{e}_{31}\varphi_0 \\ 2\bar{e}_{31}\varphi_0 \\ 0 \\ E_{31}\Phi \\ E_{31}\Phi \\ 0 \\ -E_{15}\frac{\partial \Phi}{\partial y} \\ -E_{15}\frac{\partial \Phi}{\partial x} \end{Bmatrix}^{Electerical} + \begin{Bmatrix} 2\bar{q}_{31}\psi_0 \\ 2\bar{q}_{31}\psi_0 \\ 0 \\ F_{31}\Psi \\ F_{31}\Psi \\ 0 \\ -F_{15}\frac{\partial \Psi}{\partial y} \\ -F_{15}\frac{\partial \Psi}{\partial x} \end{Bmatrix}^{Magnetic} - \begin{Bmatrix} \bar{\lambda}_{11} h\Delta T \\ \bar{\lambda}_{11} h\Delta T \\ 0 \\ 0 \\ 0 \\ 0 \\ 0 \\ 0 \end{Bmatrix}^{Thermal} - \begin{Bmatrix} \bar{\chi}_{11} h\Delta H \\ \bar{\chi}_{11} h\Delta H \\ 0 \\ 0 \\ 0 \\ 0 \\ 0 \\ 0 \end{Bmatrix}^{Hygral} \tag{44a-h}$$

Then, Eqs. (42) are used to rewrite the stress resultants in higher-order nonlocal (HON) forms:

$$\left(1 - \left(\mu_0^2 + \mu_1^2\right)\nabla^2 + \mu_0^2\mu_1^2\nabla^4\right) M_x = -\left[\left(1 - \mu_1^2\nabla^2\right) - l^2\left(1 - \mu_0^2\nabla^2\right)\nabla^2\right]\left(D_{11}\frac{\partial^2 w_0}{\partial x^2} + D_{12}\frac{\partial^2 w_0}{\partial y^2}\right) + E_{31}\Phi + F_{31}\Psi \tag{45a}$$

$$\left(1 - \left(\mu_0^2 + \mu_1^2\right)\nabla^2 + \mu_0^2\mu_1^2\nabla^4\right) M_y = -\left[\left(1 - \mu_1^2\nabla^2\right) - l^2\left(1 - \mu_0^2\nabla^2\right)\nabla^2\right]\left(D_{21}\frac{\partial^2 w_0}{\partial x^2} + D_{22}\frac{\partial^2 w_0}{\partial y^2}\right) + E_{31}\Phi + F_{31}\Psi \tag{45b}$$

$$\left(1-\left(\mu_0^2+\mu_1^2\right)\nabla^2+\mu_0^2\mu_1^2\nabla^4\right)M_{xy}=-\left[\left(1-\mu_1^2\nabla^2\right)-l^2\left(1-\mu_0^2\nabla^2\right)\nabla^2\right]\left(D_{66}\frac{\partial^2 w_0}{\partial x\,\partial y}\right)$$

(45c)

$$\left(1-\left(\mu_0^2+\mu_1^2\right)\nabla^2+\mu_0^2\mu_1^2\nabla^4\right)Q_x=\left[\left(1-\mu_1^2\nabla^2\right)-l^2\left(1-\mu_0^2\nabla^2\right)\nabla^2\right]H_{44}\left(A\frac{\partial^3 w_0}{\partial x^3}+B\frac{\partial^3 w_0}{\partial x\,\partial y^2}\right)-E_{15}\frac{\partial\Phi}{\partial x}-F_{15}\frac{\partial\Psi}{\partial x}$$

(45d)

$$\left(1-\left(\mu_0^2+\mu_1^2\right)\nabla^2+\mu_0^2\mu_1^2\nabla^4\right)Q_y=\left[\left(1-\mu_1^2\nabla^2\right)-l^2\left(1-\mu_0^2\nabla^2\right)\nabla^2\right]H_{44}\left(A\frac{\partial^3 w_0}{\partial x^2\partial y}+B\frac{\partial^3 w_0}{\partial y^3}\right)-E_{15}\frac{\partial\Phi}{\partial y}-F_{15}\frac{\partial\Psi}{\partial y}$$

(45e)

$$\left(1-\left(\mu_0^2+\mu_1^2\right)\nabla^2+\mu_0^2\mu_1^2\nabla^4\right)\begin{Bmatrix}\overline{D}_x\\ \overline{D}_y\\ \overline{D}_z\end{Bmatrix}=\begin{Bmatrix}\left[\left(1-\mu_1^2\nabla^2\right)-l^2\left(1-\mu_0^2\nabla^2\right)\nabla^2\right]E_{15}\left(A\frac{\partial^3 w_0}{\partial x^3}+B\frac{\partial^3 w_0}{\partial x\,\partial y^2}\right)+X_{11}\frac{\partial\Phi}{\partial x}+Y_{11}\frac{\partial\Psi}{\partial x}\\ \left[\left(1-\mu_1^2\nabla^2\right)-l^2\left(1-\mu_0^2\nabla^2\right)\nabla^2\right]E_{15}\left(A\frac{\partial^3 w_0}{\partial x^2\partial y}+B\frac{\partial^3 w_0}{\partial y^3}\right)+X_{11}\frac{\partial\Phi}{\partial y}+Y_{11}\frac{\partial\Psi}{\partial y}\\ -\left[\left(1-\mu_1^2\nabla^2\right)-l^2\left(1-\mu_0^2\nabla^2\right)\nabla^2\right]\left(E_{31}\frac{\partial^2 w_0}{\partial x^2}+E_{31}\frac{\partial^2 w_0}{\partial y^2}\right)-X_{33}\Phi-Y_{33}\Psi\end{Bmatrix} \quad (46a\text{-}c)$$

$$\left(1-\left(\mu_0^2+\mu_1^2\right)\nabla^2+\mu_0^2\mu_1^2\nabla^4\right)\begin{Bmatrix}\overline{B}_x\\ \overline{B}_y\\ \overline{B}_z\end{Bmatrix}=\begin{Bmatrix}\left[\left(1-\mu_1^2\nabla^2\right)-l^2\left(1-\mu_0^2\nabla^2\right)\nabla^2\right]F_{15}\left(A\frac{\partial^3 w_0}{\partial x^3}+B\frac{\partial^3 w_0}{\partial x\,\partial y^2}\right)+Y_{11}\frac{\partial\Phi}{\partial x}+Y_{22}\frac{\partial\Psi}{\partial x}\\ \left[\left(1-\mu_1^2\nabla^2\right)-l^2\left(1-\mu_0^2\nabla^2\right)\nabla^2\right]F_{15}\left(A\frac{\partial^3 w_0}{\partial x^2\partial y}+B\frac{\partial^3 w_0}{\partial y^3}\right)+Y_{11}\frac{\partial\Phi}{\partial y}+Y_{22}\frac{\partial\Psi}{\partial x}\\ -\left[\left(1-\mu_1^2\nabla^2\right)-l^2\left(1-\mu_0^2\nabla^2\right)\nabla^2\right]\left(F_{31}\frac{\partial^2 w_0}{\partial x^2}+F_{31}\frac{\partial^2 w_0}{\partial y^2}\right)-Y_{33}\Phi-Y_{44}\Psi\end{Bmatrix} \quad (47a\text{-}c)$$

Now, incorporating the Eqs. (37) and Eqs. (45-47) and then inserting them into Eqs. (28), the hygro-thermo-electro-magneto-mechanical stability equations would be obtained.

3. Analytical approaches

3.1 Navier's solution (A-I)

In this subsection, the double series solution is employed in order to apply simple boundary condition and solve the stability equations. This method considers the dependency of displacement field of in-plane coordinates as a set of harmonic sentences (sinusoidal series). This dependency had to be formed in such a way as to satisfy the essential boundary conditions (BCs).

Mathematically, the differential equations are of order 2*n*, the conditions of order *0* to *n-1* are essential and the conditions of order *n* to *2n-1* are natural. The essential BCs are imposed directly in the solution imposed by the trial functions, which eventually are required to satisfy them. The natural BCs are imposed in the right hand side of the resulting system $K_{ij} \times U_j = F_{ij}$ (in which K is matrix of coefficients, F is vector of forces and U is set of displacements) and they are not necessarily satisfied by the trial functions. Indeed, they cannot be prescribed and with the use of the essential BCs, these are not needed in the solution [76]. Here, an investigation on the order of higher-order nonlocal strain gradient based-stability equations shows the conditions with orders from zero to four are essential BCs to solve present equations (order=10, n=5).

For bending moments M_x and M_y, the order is ten (Eqs. (45)) and would be natural BCs. To the best of the authors' knowledge, for some numerical solutions such as the differential quadrature method (DQM) in some special cases, there have been required to have some additional BCs which should be directly conjugated to the equations because of equalizing the number of unknowns with the number of equations [77]. The Navier's method assumes the solution as a sum of mode shapes (X_m and Y_n) of the plate which automatically satisfies all the essential BCs (Eqs. (48)). However, the BCs in Eqs. 50 are stayed as natural BCs due to their orders and the Navier's approach cannot directly satisfy them for the OVFSDT. In conclusion, the natural BCs in some special cases can never be exactly satisfied by solutions with variables separable such as Navier's, Ritz's and or others [78].

First of all, the essential and natural BCs would be listed in the following sections:

A) Essential BCs according to higher-order nonlocal strain gradient-based OVFSDT governing equations:

Simply-supported:

$$\Phi(0, y) = \Phi(L_x, y) = 0; \Psi(0, y) = \Psi(L_x, y) = 0; w_0(0, y) = w_0(L_x, y) = 0 \quad (48a)$$

$$\Phi(x, 0) = \Phi(x, L_y) = 0; \Psi(x, 0) = \Psi(x, L_y) = 0; w_0(x, 0) = w_0(x, L_y) = 0 \quad (48b)$$

Clamped:

$$\Phi(0, y) = \Phi(L_x, y) = 0; \Psi(0, y) = \Psi(L_x, y) = 0; w_0(0, y) = w_0(L_x, y) = 0 \quad (49a)$$

$$\Phi(x, 0) = \Phi(x, L_y) = 0; \Psi(x, 0) = \Psi(x, L_y) = 0; w_0(x, 0) = w_0(x, L_y) = 0 \quad (49b)$$

B) Natural BCs according to higher-order nonlocal strain gradient-based OVFSDT governing equations:

Simply-supported:

$Mx\ (x, 0) = Mx\ (x, Ly) = 0$ (50a)

$My\ (0, y) = My\ (Lx, y) = 0$ (50b)

Free:

$Mx\ (x, 0) = Mx\ (x, Ly) = 0$ (51a)

$My\ (0, y) = My\ (Lx, y) = 0$ (51b)

$Mxy\ (x, 0) = Mxy\ (x, Ly) = 0$ (51c)

$Mxy\ (0, y) = Mxy\ (Lx, y) = 0$ (51d)

$Qx\ (x, 0) = Qx\ (x, Ly) = 0$ (51e)

$Qy\ (0, y) = Qy\ (Lx, y) = 0$ (51f)

And also the local BCs computed from calculus of variations are presented as follows:

$$\int_0^{Lx}\left(\begin{array}{l} A\dfrac{\partial^2 Q_y}{\partial x^2}+B\dfrac{\partial^2 Q_y}{\partial y^2}+\dfrac{\partial M_y}{\partial y}+2\dfrac{\partial M_{xy}}{\partial x}+ \\ N_y\left(\dfrac{\partial w_0}{\partial y}+B^2\dfrac{\partial^5 w_0}{\partial y^5}+A^2\dfrac{\partial^5 w_0}{\partial x^4\partial y}+2B\dfrac{\partial^3 w_0}{\partial y^3}+2AB\dfrac{\partial^5 w_0}{\partial x^2\partial y^3}+2A\dfrac{\partial^3 w_0}{\partial x^2\partial y}\right) \end{array}\right)dx \quad (52a)$$

$$\int_0^{Ly}\left(\begin{array}{l} A\dfrac{\partial^2 Q_x}{\partial x^2}+B\dfrac{\partial^2 Q_x}{\partial y^2}+\dfrac{\partial M_x}{\partial x}+N_{xy}\dfrac{\partial w_0}{\partial y}+ \\ N_x\left(\dfrac{\partial w_0}{\partial x}+A^2\dfrac{\partial^5 w_0}{\partial x^5}+B^2\dfrac{\partial^5 w_0}{\partial x\,\partial y^4}+2A\dfrac{\partial^3 w_0}{\partial x^3}+2AB\dfrac{\partial^5 w_0}{\partial x^3\partial y^2}+2B\dfrac{\partial^3 w_0}{\partial x\,\partial y^2}\right) \end{array}\right)dy \quad (52b)$$

Here, the displacement field and potential functions utilizing Navier's approach can be expanded in the following forms [47]:

$$w_0=\sum_{m=1}^{\infty}\sum_{n=1}^{\infty}W_{0mn}X_m(x)Y_n(y) \quad (53a)$$

$$\Phi=\sum_{m=1}^{\infty}\sum_{n=1}^{\infty}\Phi_{0mn}X_m(x)Y_n(y) \quad (53b)$$

$$\Psi=\sum_{m=1}^{\infty}\sum_{n=1}^{\infty}\Psi_{0mn}X_m(x)Y_n(y) \quad (53c)$$

In which W_{0mn}, Φ_{0mn}, and Ψ_{0mn} are the displacement and potentials unknown variables. The mode shapes to satisfy essential simply-supported boundary conditions are selected as follows [54]:

$$X_m(x) = \sin(\frac{m\pi}{L_x}x) \tag{54a}$$

$$Y_n(y) = \sin(\frac{n\pi}{L_y}y) \tag{54b}$$

Functions $X_m(x)$ and $Y_n(y)$ represent ideally the buckled shape when the number of half-waves in x and y directions are m and n. Substituting Eqs. (54) into stability equations, the algebraic equations can be obtained:

$$\begin{Bmatrix} K_{11} & K_{12} & K_{13} \\ K_{21} & K_{22} & K_{23} \\ K_{31} & K_{32} & K_{33} \end{Bmatrix} \begin{Bmatrix} W_{0mn} \\ \Phi_{0mn} \\ \Psi_{0mn} \end{Bmatrix} = 0 \tag{55}$$

The coefficients K_{ij} (i, j=1, 2, 3) are extracted in the Appendix A.

3.2 Galerkin's integral method (A-II)

Another analytical solution is considered to implement various boundary conditions in the Table 1 [25, 47].

Table 1. Various admissible and suitable functions by which all of the essential boundary conditions could be satisfied [25, 47].

Boundary conditions					The function $X_m(x)$ and $Y_n(y)$	
Notation	x=0	y=0	x=L_x	y=L_y	$X_m(x)$	$Y_n(y)$
SSSS	S	S	S	S	$\sin(\frac{m\pi}{L_x}x)$	$\sin(\frac{n\pi}{L_y}y)$
CCCC	C	C	C	C	$\sin^2(\frac{m\pi}{L_x}x)$	$\sin^2(\frac{n\pi}{L_y}y)$
SCSC	S	C	S	C	$\sin(\frac{m\pi}{L_x}x)$	$\sin^2(\frac{n\pi}{L_y}y)$
CSCS	C	S	C	S	$\sin^2(\frac{m\pi}{L_x}x)$	$\sin(\frac{n\pi}{L_y}y)$
SFSF	S	F	S	F	$\sin(\frac{m\pi}{L_x}x)$	$\left[\sin^2(\frac{n\pi}{L_y}y)+1\right]\cos^2(\frac{n\pi}{L_y}y)$

FSFS	F	S	F	S	$\left[\sin^2(\frac{m\pi}{L_x}x)+1\right]\cos^2(\frac{m\pi}{L_x}x)$	$\sin(\frac{n\pi}{L_y}y)$
CFCF	C	F	C	F	$\sin^2(\frac{m\pi}{L_x}x)$	$\left[\sin^2(\frac{n\pi}{L_y}y)+1\right]\cos^2(\frac{n\pi}{L_y}y)$
FCFC	F	C	F	C	$\left[\sin^2(\frac{m\pi}{L_x}x)+1\right]\cos^2(\frac{m\pi}{L_x}x)$	$\sin^2(\frac{n\pi}{L_y}y)$

Now by substituting X_m (x) and Y_n (y) into stability equations, the algebraic equations would be obtained:

$$\begin{Bmatrix} R_{11} & R_{12} & R_{13} \\ R_{21} & R_{22} & R_{23} \\ R_{31} & R_{32} & R_{33} \end{Bmatrix} \begin{Bmatrix} W_{0mn} \\ \Phi_{0mn} \\ \Psi_{0mn} \end{Bmatrix} = 0 \tag{56}$$

The coefficients R_{ij} (i, j=1, 2, 3) are expanded in the Appendix B.

To solve the Eqs. (55, 56), the determinant of the matrix of K_{ij} and R_{ij} must be set to zero. By doing so and after some algebraic manipulation, the critical buckling load is obtained.

4. Numerical results

First of all, the accuracy of the numerical results originated from the OVFSDT had to be compared and validated against other theories. In particular, it is very important to understand what the difference is made between the results of different theories. Table 2 presents critical buckling loads of nanoplates collated from several well-known references [79-81] ranging from the FSDT, S-FSDT and molecular dynamics simulation (MD); these are compared with results obtained by the new theory, namely OVFSDT, proposed in this paper. It is clearly seen that the results of critical buckling load with an increase in length value of the plate are closer to MD outcomes. Generally, Table 2 shows the close numerical results between the present theory and others from which the theory could be approved. Further comparisons are shown in Table 3 where the present OVFSDT's biaxial buckling loads are validated against those obtained by the DQM [80] and the MD [81]. In the Table 3, the amounts have further differences versus Table 2; however, there is an adaptable agreement and the accuracy of the new theory is confirmed.

In order to have a comparison for critical buckling loads of the PMEN, buckling results of the PMEN obtained by utilizing various plate theories as calculated in ref [17] are illustrated. The critical buckling load considered as a non-dimensional factor corresponding to various length-to-thickness ratios and non-dimensional lower-order nonlocal (LON) parameters for fully simply-supported boundary conditions are tabulated in Table 4. As shown in the Table, the non-dimensional critical buckling loads computed by the current plate theory are in excellent agreement with those given in [17]. For the larger amounts of the nonlocal parameter, the difference between the critical buckling loads of present study with those predicted by [17] are becoming smaller and smaller. This is because the nonlocal parameter reduced external impacts whether they are mechanical or non-mechanical forces. On the other hand, for the thin PMEN, the difference between results is negligible in contrast to those of moderately thick plates between local and nonlocal analyses. These confirm that the new theory proposed in this study is able to gain appropriate and accurate results by carrying out and refining the errors, despite the fact that developing a complete theory is not within the scope of this study.

Table 2. Results of buckling loads for a nanoplate developed from the DQM [79-80], and the MD simulation [81].

E=1TPa, υ=0.16, k_s=5/6, μ=1.81nm^2, SSSS

Biaxial buckling load (*nN/nm*)					
Present		FSDT-DQM	FSDT-DQM	MD results	*Lx=Ly*
A-I	A-II	[79]	[80]	[81]	*(nm)*
1.02740	1.09473	1.0749	1.0809	1.0837	4.99
0.62151	0.66171	0.6523	0.6519	0.6536	8.080
0.43832	0.41208	0.4356	0.4350	0.4331	10.77
0.26122	0.26969	0.2645	0.2639	0.2609	14.65
0.17075	0.17168	0.1751	0.1748	0.1714	18.51
0.11963	0.12009	0.1239	0.1237	0.1191	22.35
0.08856	0.08808	0.0917	0.0914	0.0889	26.22
0.06918	0.06925	0.0707	0.0705	0.0691	30.04
0.05568	0.05579	0.0561	0.0560	0.0554	33.85
0.04488	0.04453	0.0453	0.0451	0.0449	37.81

Table 3. Results of biaxial buckling loads and comparisons with the DQM [80] and the MD [81] for a nanoplate.

E=1TPa, υ=0.16, k_s=5/6, μ=1.81nm^2, SSSS

Biaxial buckling load (*nN/nm*)

Present		FSDT [80]	MD results [81]	*Lx/Ly*
A-I	A-II			
0.52449	0.50894	0.5115	0.5101	0.5
0.56223	0.54239	0.5715	0.5693	0.75
0.64225	0.62217	0.6622	0.6595	1.25
0.75576	0.81835	0.7773	0.7741	1.5
1.01340	1.06650	1.0222	1.0183	1.75
1.17030	1.14031	1.1349	1.1297	2

Table 4. Comparisons of the non-dimensional biaxial critical buckling loads of fully simply-supported the PMEN computed by various plate theories ($h=10$ *nm,* $\varphi_0=-0.3$ *V,* $\psi_0=0.01$ *A,* $\Delta T=100$ *K,* $\Gamma_0=\mu_0/L_x, P_0 = N_0 / A_{11}$) [17].

Non-dimensional biaxial buckling load (P_0)							
L_x/h	Reference	Theory	Non-dimensional nonlocal parameter (Γ_0)				
			0	0.01	0.02	0.03	0.04
8	Present, OVFSDT, ENET[*1]	A-I	21.4653	21.4586	21.3995	21.2211	20.9757
		A-II	21.6211	21.5741	21.4542	21.2746	21.0980
	[17]-ENET[*1]	KPT[*2]	23.9006	23.8593	23.7365	23.5349	23.2592
		MPT[*3]	21.8250	21.7877	21.6768	21.4948	21.2459
		RPT[*4]	21.8447	21.8074	21.6963	21.5141	21.2648
		PSDPT[*5]	21.8393	21.8020	21.6910	21.5088	21.2596
		TSDPT[*6]	21.8489	21.8116	21.7006	21.5183	21.2690
		HSDPT[*7]	21.8666	21.8294	21.7187	21.5370	21.2885
		ESDPT[*8]	21.8589	21.8216	21.7105	21.5282	21.2787
12	Present	A-I	26.7203	26.6820	26.5618	26.3590	26.1315
		A-II	26.6210	26.5818	26.4751	26.2736	26.0120
	[17]	KPT	27.6888	27.6475	27.5245	27.3228	27.0469
		MPT	26.6753	26.6360	26.5191	26.3273	26.0650
		RPT	26.6842	26.6449	26.5280	26.3361	26.0737
		PSDPT	26.6817	26.6425	26.5255	26.3337	26.0712
		TSDPT	26.6862	26.6469	26.5299	26.3380	26.0756
		HSDPT	26.6946	26.6553	26.5384	26.3466	26.0843
		ESDPT	26.6908	26.6515	26.5346	26.3426	26.0801
20	Present	A-I	39.7291	39.5684	39.4276	39.1298	38.8589
		A-II	39.5855	39.4254	39.3049	39.0978	38.8273
	[17]	KPT	39.8097	39.7683	39.6450	39.4427	39.1661
		MPT	39.3684	39.3280	39.2078	39.0106	38.7408
		RPT	39.3719	39.3315	39.2112	39.0140	38.7441
		PSDPT	39.3709	39.3305	39.2103	39.0130	38.7432
		TSDPT	39.3726	39.3322	39.2120	39.0147	38.7449
		HSDPT	39.3787	39.3389	39.2213	39.7208	38.7752
		ESDPT	39.3744	39.3340	39.2138	39.0165	38.7466
30	Present	A-I	44.8205	44.7622	44.6527	44.5038	44.2281
		A-II	44.8894	44.8291	44.7089	44.5117	44.2421
	[17]	KPT	45.9379	44.8576	44.7635	44.5699	44.4315
		MPT	44.9031	44.8627	44.7425	44.5453	44.2755
		RPT	44.9067	44.8663	44.7460	44.5488	44.2790
		PSDPT	44.9057	44.8653	44.7451	44.5478	44.2780
		TSDPT	44.9074	44.8670	44.7468	44.5496	44.2797
		HSDPT	44.9137	44.8741	44.7577	44.5599	44.2949
		ESDPT	44.9093	44.8689	44.7487	44.5514	44.2816

[1] Eringen's nonlocal elasticity theory ($\Gamma_0 \neq 0, \Gamma_1 = 0, l = 0$)
[2] Kirchhoff's plate theory
[3] Mindlin's plate theory
[4] Reddy's plate theory
[5] Parabolic shear deformable plate theory
[6] Trigonometric shear deformable plate theory
[7] Hyperbolic shear deformable plate theory
[8] Exponential shear deformable plate theory

Table 5. Properties of Barium titanate–cobalt ferrite composite ceramic nanoplate [16-18, 82-85]

$BaTiO_3$-$CoFe_2O_4$	Elastic properties (*GPa*)
	$C_{11}=C_{22}=226$, $C_{12}=125$, $C_{13}=C_{23}=124$, $C_{33}=216$, $C_{44}=C_{55}=44.2$, $C_{66}=50.5$
	Piezoelectric quantities (C/m^2)
	$e_{31}=e_{32}=-2.2$, $e_{15}=e_{24}=5.8$, $e_{33}=9.3$
	Dielectric quantities ($C/V.m$)
	$\kappa_{11}=\kappa_{22}=5.64e\text{-}9$, $\kappa_{33}=6.35e\text{-}9$
	Piezomagnetic quantities ($N/A.m$)
	$q_{31}=q_{32}=290.1$, $q_{33}=349.9$, $q_{15}=275$
	Magnetoelectric quantities ($N.s/V.C$)
	$d_{11}=d_{22}=5.367e\text{-}12$, $d_{33}=2737.5e\text{-}12$
	Magnetic quantities ($N.s^2/C^2$)
	$\eta_{11}=\eta_{22}=-297e\text{-}6$, $\eta_{33}=83.5e\text{-}6$
	Thermal modulus ($N/m^2.K$)
	$\lambda_{11}=\lambda_{22}=4.738e5$, $\lambda_{33}=4.529e5$,
	Pyroelectric quantities (C/N)
	$p_1=p_2=p_3=0.25e\text{-}4$
	Hygral expansion coefficient
	$\chi_{11}=3.5939\left(w\ t.\%H_2O\right)^{-1}$
	$\chi_{33}=64.355\left(w\ t.\%H_2O\right)^{-1}$
	Other quantities
	$h=4nm$, $Lx=Ly=60nm$, $k_W=1.13GPa/nm$, $k_G=1.13Pa.m$, $P_0=N^0/A_{11}$, $l^*=l/h$, $\beta=L_x/L_y$

To show the behavior of the half-waves, Figs. 2a-d are examined for A-I and A-II solutions. Fig. 2a represents the shape of the half-waves within which the curves are similar to trigonometric ones. In fact,

the curves in this figure are the responses of the solutions in such a situation and every point on the curves can be an answer of those solutions and therefore the curves include the exact result. By considering Figs. 2b and 2c, it is observed that if β is larger than 1, the critical load can decrease or increase with the plate length. By attending to Fig. 2d, it can be mentioned that the results of A-II are smaller than the A-I in these cases; however, both of them are in excellent agreements to each other.

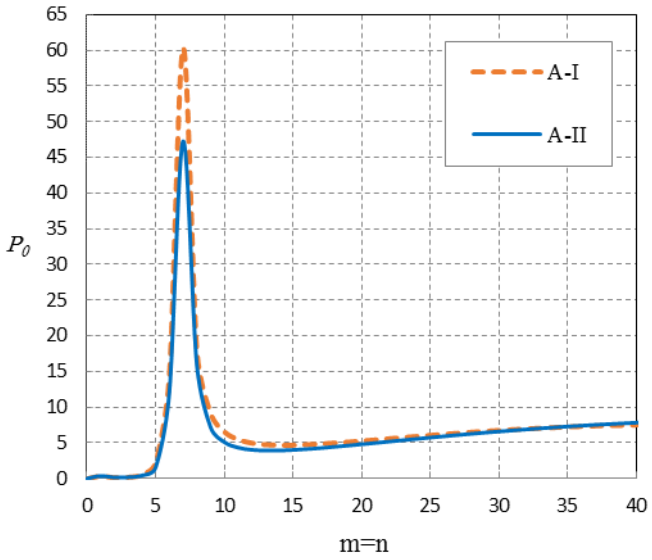

Fig. 2a. The number of half-waves versus different analytical solutions (μ_0= 0.2 nm, μ_1= 0.4 nm, l=0.5h, φ_0=0.01 V, ψ_0=0.1 A, H_y=40%, Ly=60nm, β=1, ΔT=400 K, SSSS)

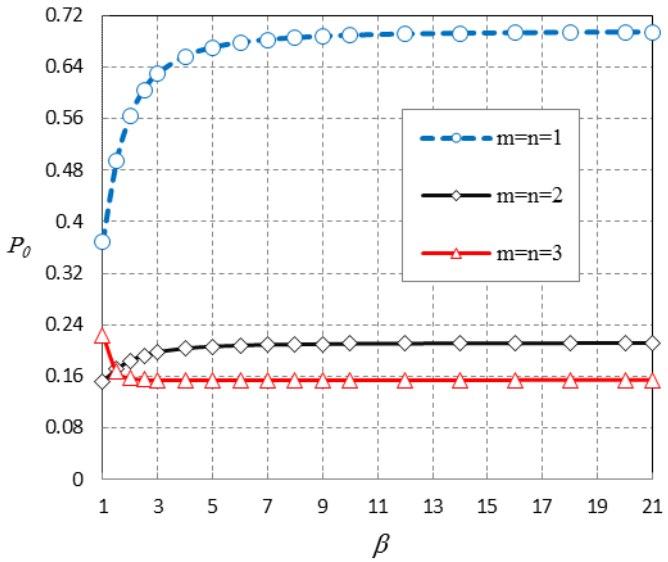

Fig. 2b. The number of half-waves versus different aspect ratios (μ_0= 0.2 nm, μ_1= 0.4 nm, l=0.5h, φ_0=0.01 V, ψ_0=0.1 A, H_y=40%, Ly=60nm, ΔT=400 K, A-I, SSSS)

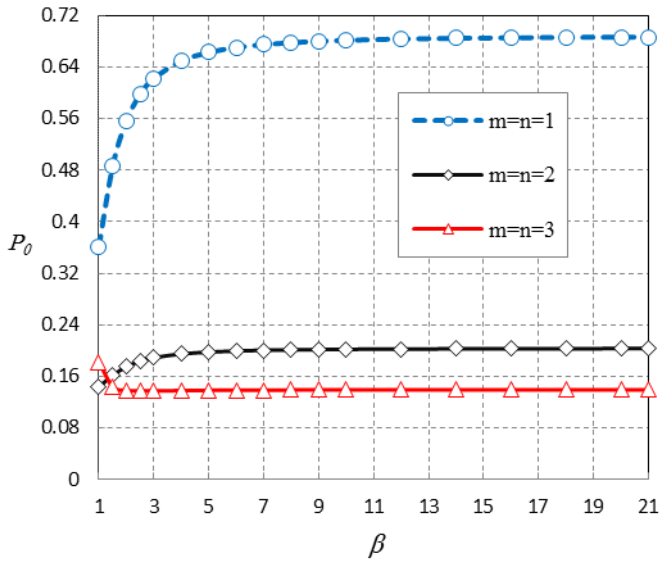

Fig. 2c. The number of half-waves versus different aspect ratios (μ_0= *0.2 nm,* μ_1= *0.4 nm, l=0.5h,* φ_0*=0.01 V,* ψ_0*=0.1 A,* H_y*=40%, Ly=60nm,* ΔT*=400 K, A-II, SSSS)*

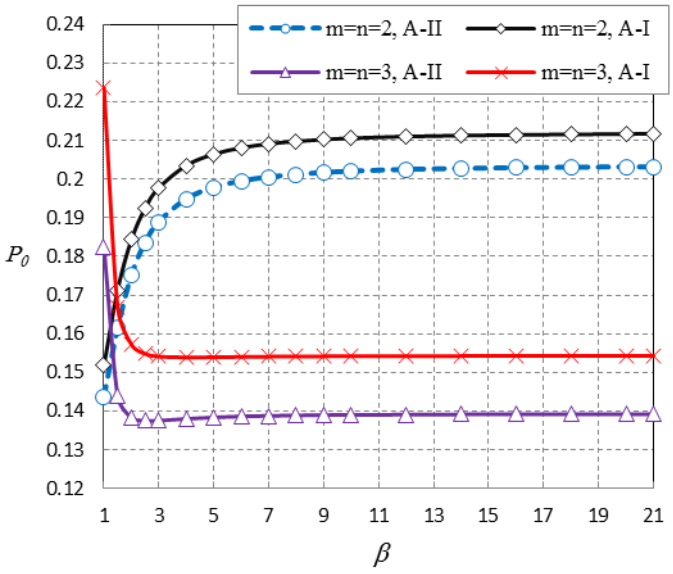

Fig. 2d. The number of half-waves versus different aspect ratios (μ_0= *0.2 nm,* μ_1= *0.4 nm, l=0.5h,* φ_0*=0.01 V,* ψ_0*=0.1 A,* H_y*=40%, Ly=60nm,* ΔT*=400 K, SSSS)*

Figs. 3a and b depict the SGLS factor versus several Winkler elastic foundation values by assuming medium hygral and ΔT*=400 K*; such a temperature is chosen because it was unable to enter to much higher heat due to unpredictable thermal buckling occurring in great temperatures. As expected, by growing SGLS parameter, the stiffness-hardening of the size-dependent plate increased [25]. As it is shown, the buckling load is declining when the elastic substrate is removed. This outcome could be reversed while the matrix is appeared. Hence, the significance of foundation used is vividly illustrated

through this figure. It can be further observed that the absence and presence of the foundation in m=n=1 are more tangible than m=n=2.

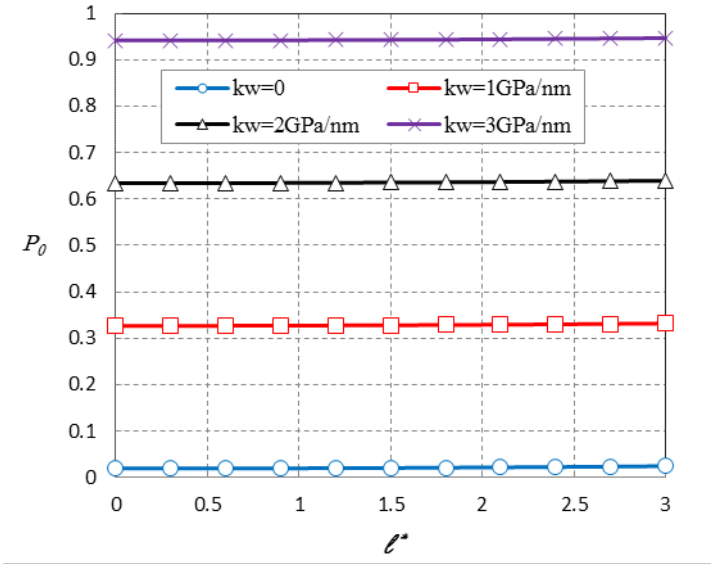

Fig. 3a. The SGLS parameter versus different Winkler coefficients (μ_0=0.5 nm, μ_1=0.1 nm, φ_0=0.1 V, ψ_0=0.1 A, ΔT=400 K, H_y=40%, m=n=1, β=1, A-I, k_G=1.13GPa, SSSS)

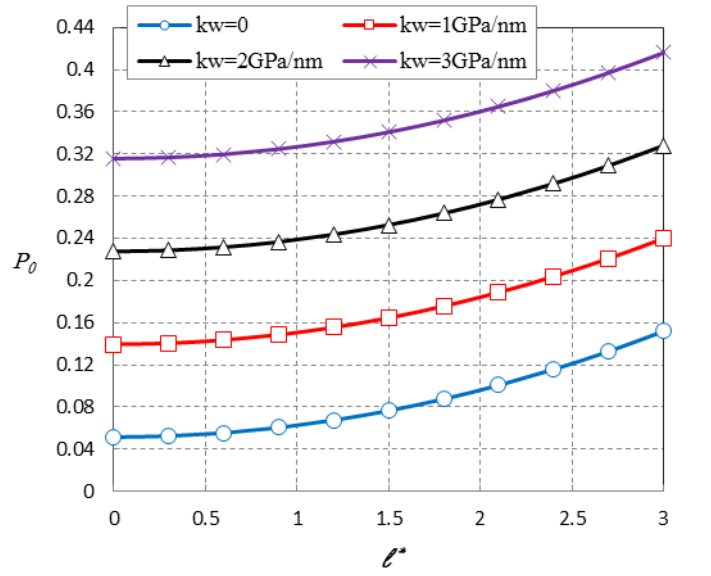

Fig. 3b. The SGLS parameter versus different Winkler coefficients (μ_0=0.5 nm, μ_1=0.1 nm, φ_0=0.1 V, ψ_0=0.1 A, ΔT=400 K, H_y=40%, m=n=2, β=1, A-I, k_G=1.13GPa, SSSS)

To consider several situations of nonlocality for electric and magnetic potentials Figs. 4a-e are displayed. The major aim of these figures is to compare the important conditions as described below. First off, HON parameter has been investigated by exerting various exterior electric voltages in solution A-II for two half-waves. As can be seen in Fig. 4a, with an increase in the external electric voltage, critical buckling loads are slowly reducing; however, this trend for m=n=2 in Fig. 4b is more

appreciable. Fig. 4c reveals HON parameter impact on several boundary conditions. It can be proved that in A-II the other boundary conditions have more decreasing effect versus SSSS in m=n=1. On the whole, the conditions with clamped boundaries have been further impressed by HON parameter which can be seen in FCFC, CFCF and CCCC, respectively. The graphs in Figs. 4d and 4e are plotted for A-I which show the same behavior with Figs. 4a and 4b, namely, increasing electric voltage decreasing critical buckling loads, but that diminish influence is not as much as the decreasing effect of the HON parameter on the critical buckling loads. Generally, the HON parameter in A-II solution has further decreasing effect versus A-I on the outcomes.

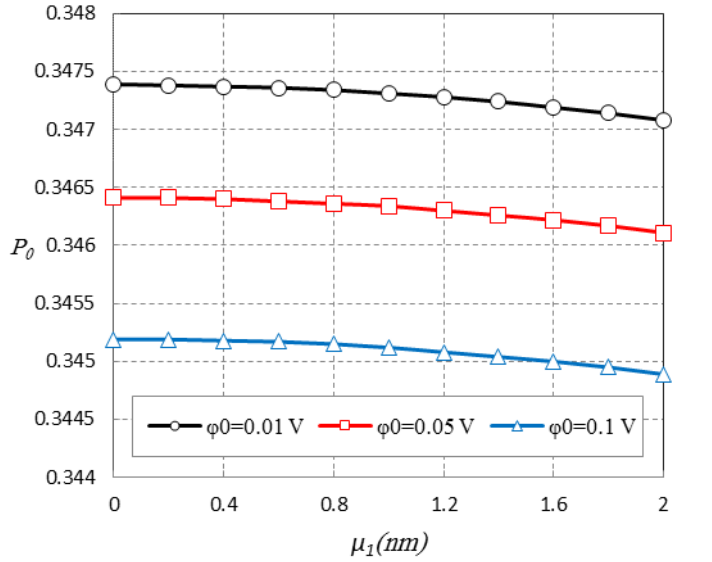

Fig. 4a. The HON parameter versus different external electric voltage (μ_0*=0.2 nm, l=0.5h,* ψ_0*=0.05 A,* ΔT*=400 K,* H_y*=40%, m=n=1,* β*=1, A-II, SSSS*)

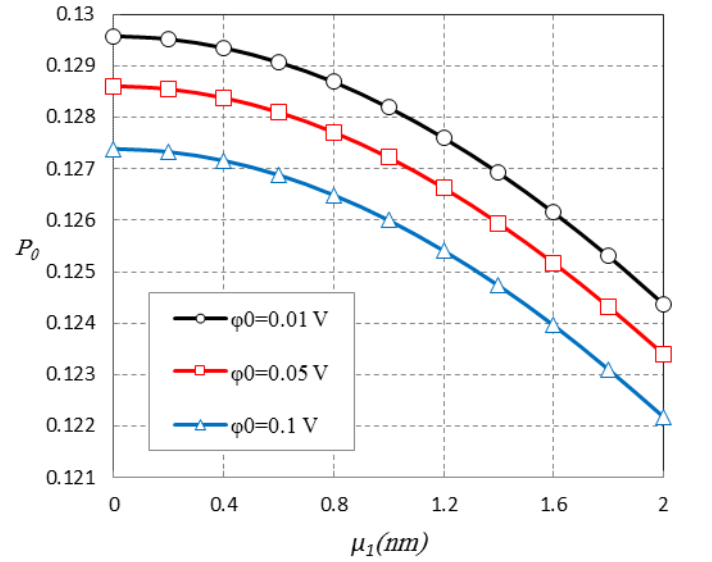

Fig. 4b. The HON parameter versus different external electric voltage (μ_0=0.2 nm, l=0.5h, ψ_0=0.05 A, ΔT=400 K, H_y=40%, m=n=2, β=1, A-II, SSSS)

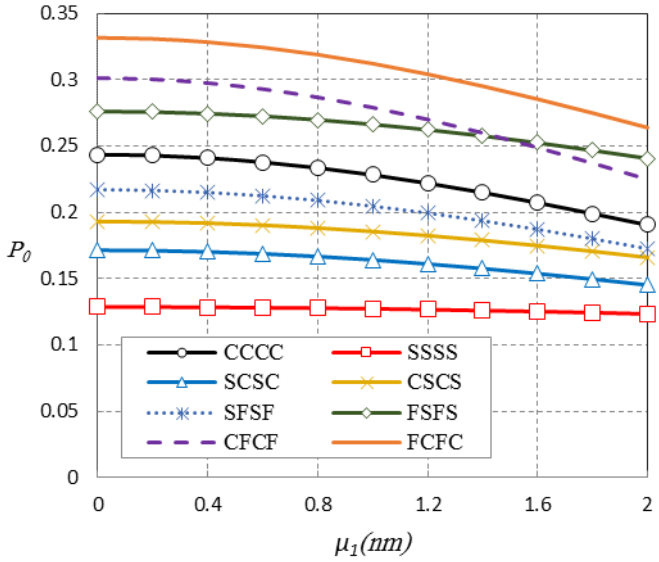

Fig. 4c. The HON parameter versus several boundary conditions (μ_0=0.2 nm, l=0.5h, φ_0=0.05 V, ψ_0=0.05 A, ΔT=400 K, H_y=40%, m=n=2, β=1, A-II)

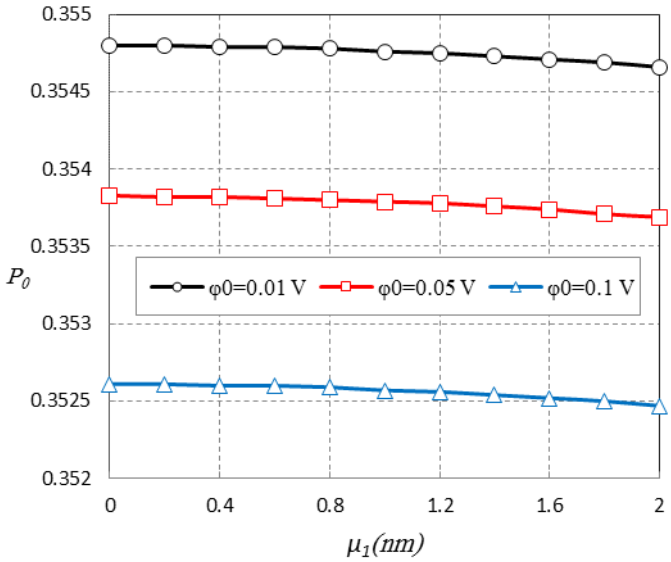

Fig. 4d. The HON parameter versus different external electric voltage (μ_0=0.2 nm, l=0.5h, ψ_0=0.05 A, ΔT=400 K, H_y=40%, m=n=1, β=1, A-I, SSSS)

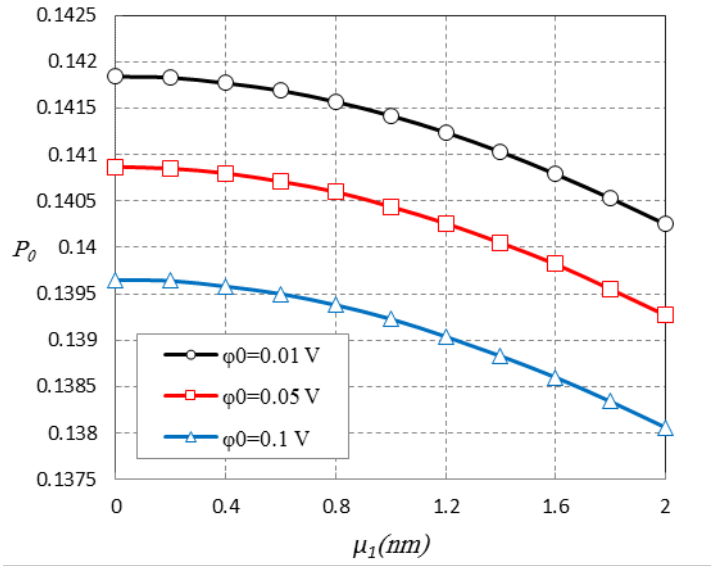

Fig. 4e. The HON parameter versus different external electric voltage (μ_0=0.2 nm, l=0.5h, ψ_0=0.05 A, ΔT=400 K, H_y=40%, m=n=2, β=1, A-I, SSSS)

Figs. 5a-d show evaluation of characteristic situations by which ENET has been reviewed due to μ_1=l=0 nm. It can be seen that the numerical values in Fig. 5b are lower than the Fig. 4e which lead to the conclusion that the use of HONSG theory increased the stiffness of the nanoplate. Although the presence of the SGLS factor might increase the stiffness, the HON parameter has considerable influences. Observations from Fig. 5a and 5c which represent the changes in the external magnetic potential show the profound impact of magnetic field versus electric one in Figs. 4 in light of the distances of the results. In fact, the difference between the critical buckling loads when the magnetic potential is considered, is much more than when the external electric potential is evaluated. Thus, it can be stated that the magnetic potential influences are much more than the electric potential effects on the critical buckling load. Fig. 5d illustrates the same result with Fig. 4c in which the greater amplitude for critical buckling loads are for boundary conditions with clamped edges by changes in LON.

It is worth noting that increasing the magnetic potential increases critical buckling loads; this is very different to the results of changing the electric potential which could be an attractive consequence. It is well-known that the carrier of all forces within the atoms is electromagnetic, so, the coupled electromagnetic potential affects the bonds between atoms and leads to softening or hardening of the nanoplate. The electromagnetic force emits two forms of electric force and magnetic one, which are two

different aspects of one thing (electromagnetic force) and therefore inherently related to each other. In the current model the material used is a ferromagnetic material (presence of Fe and Co); and in such a material, vectors of magnetic moments are isometric and tend to be aligned, so this material is highly magnetized by applying a small magnetic field. As the hardness of the model increased with enlarging magnetic field, it can be claimed that the vectors of magnetic moments do not tend to align with displacement vectors of the nanoplate's atoms which result in increasing critical buckling loads with an increase in the magnetic parameter.

The effects of the nanoplate's crystals for converting the electrical energy into deformation is lower than magnetic energy. This means that the crystals can absorb magnetic energy further than electric one leads to be more impressed by magnetic field. As an physical interpretation, after applying a potential difference on the two opposite faces of the model (e.g. top and bottom) the faces of cell of crystals have asymmetrical behavior which produce electric moments within which the model is deformed. Hereon, the external electric field as a compatible and actuator factor helps to change the deflection of the plate, which naturally leads to a rise in deflection values and leads to a reduction in critical buckling loads in stability analyzes.

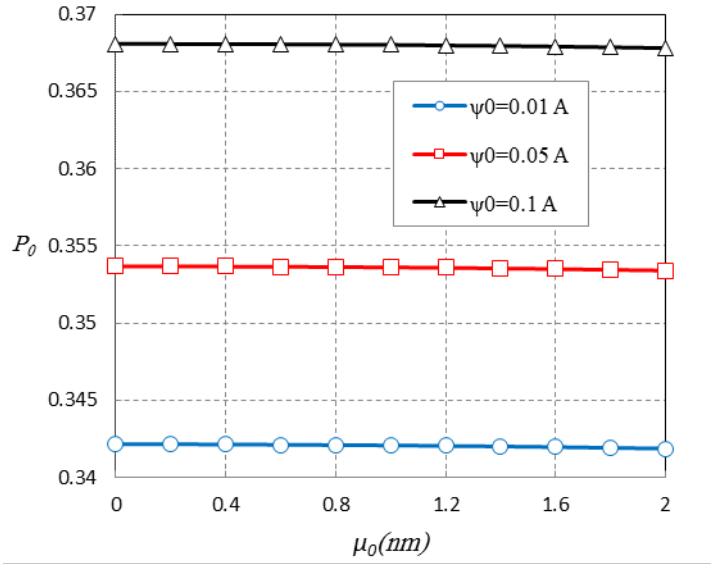

Fig. 5a. The LON parameter versus different external magnetic potential ($\mu_1=l=0$ *nm,* $\varphi_0=0.05$ *V,* $\Delta T=400$ *K,* $H_y=40\%$*,* $m=n=1$*,* $\beta=1$*,* A-I*, SSSS)*

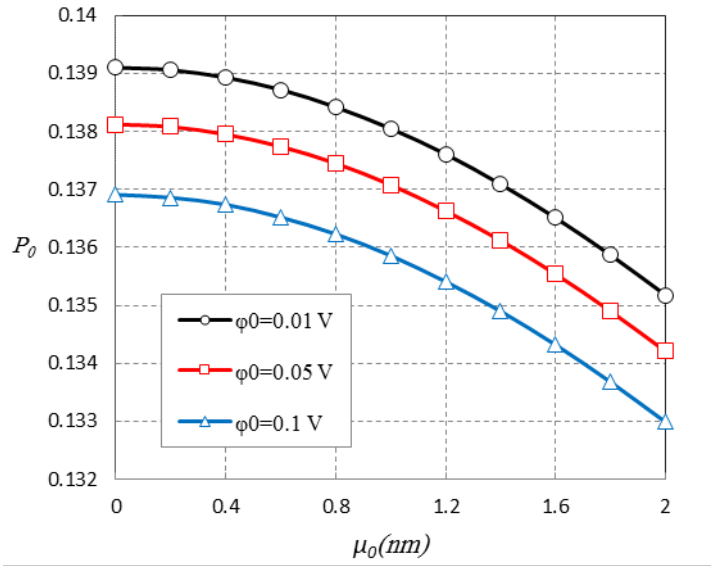

Fig. 5b. The LON parameter versus different external electric voltage ($\mu_1=l=0$ *nm,* $\psi_0=0.05$ *A,* $\Delta T=400$ *K,* $H_y=40\%$*,* $m=n=2$*,* $\beta=1$*, A-I, SSSS*)

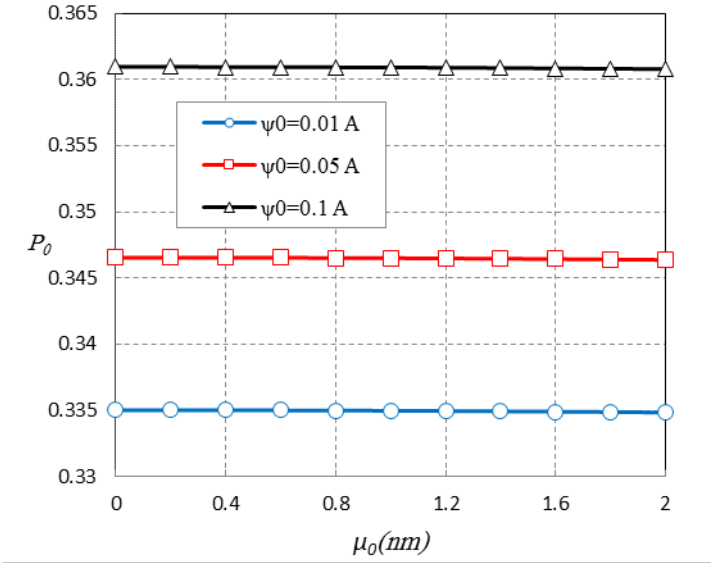

Fig. 5c. The LON parameter versus different external magnetic potential ($\mu_1=l=0$ *nm,* $\varphi_0=0.05$ *V,* $\Delta T=400$ *K,* $H_y=40\%$*,* $m=n=1$*,* $\beta=1$*, A-II, SSSS*)

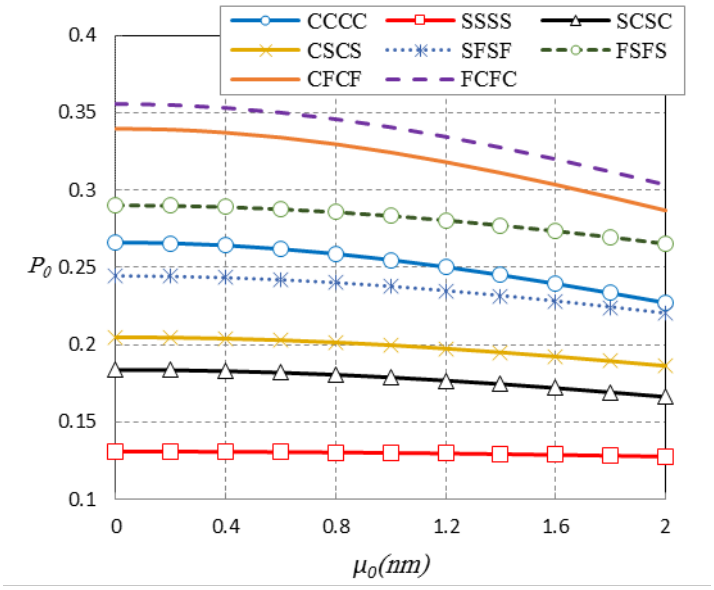

Fig. 5d. The LON parameter versus different boundary conditions ($\mu_1=l=0$ *nm*, $\varphi_0=0.05$ *V*, $\psi_0=0.05$ *A*, $\Delta T=400$ *K*, $H_y=40\%$, $m=n=2$, $\beta=1$, *A-II*)

Fig. 6a-f indicate the condition of LONSG theory by a change in electric and magnetic potentials. Initially, by comparing Fig. 5b with Fig. 6b, it is noted that the LONSG condition ($\mu_0=\mu_1=\mu$, $l\neq0$) has bigger amplitude and this is contrary to the ENET condition ($\mu_0\neq0$, $\mu_1=l=0$ *nm*), indicating that the LONSG case has more impacted on the critical buckling loads of the nanoplate subjected to electric and magnetic potentials. As a matter of fact, this is because of the large range of the results (e.g. $\varphi_0=0.05$ *V*, Fig. 5b; from 0.13812 to 0.13421, Fig. 6b; from 0.13857 to 0.13386) which clearly illustrated the major conclusion that the decrease of critical buckling loads by increasing LON parameter under LONSG condition would be further than the decrease of critical buckling loads by growing LON parameter under ENET condition. Although, the value 0.13857 in condition $l=0.2h$, $\mu=0$ is bigger than the condition $l=\mu_0=\mu_1=0$ (0.13812) in light of the SGLS parameter, the value of 0.13386 in condition $l=0.2h$, $\mu=2nm$ is smaller than 0.13421 ($\mu_0=2nm$, $\mu_1=0$, $l=0$) which proves the claim.

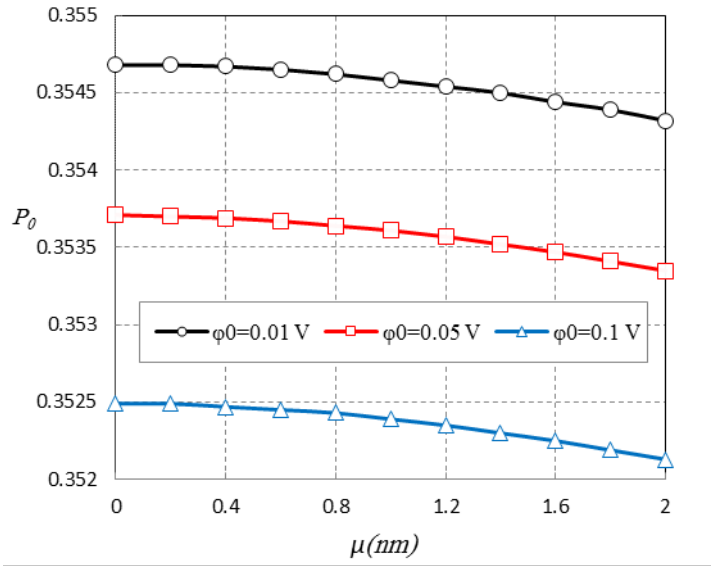

Fig. 6a. The LONSG condition versus different external electric voltage ($\mu_0 = \mu_1 = \mu$, $l=0.2h$, $\psi_0=0.05$ *A*, $\Delta T=400$ *K*, $H_y=40\%$, $m=n=1$, $\beta=1$, *A-I, SSSS)*

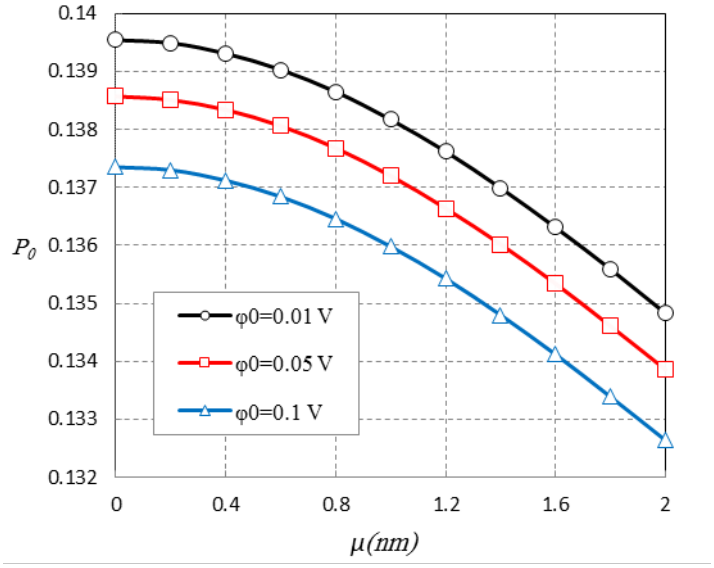

Fig. 6b. The LONSG condition versus different external electric voltage ($\mu_0 = \mu_1 = \mu$, $l=0.2h$, $\psi_0=0.05$ *A*, $\Delta T=400$ *K*, $H_y=40\%$, $m=n=2$, $\beta=1$, *A-I, SSSS)*

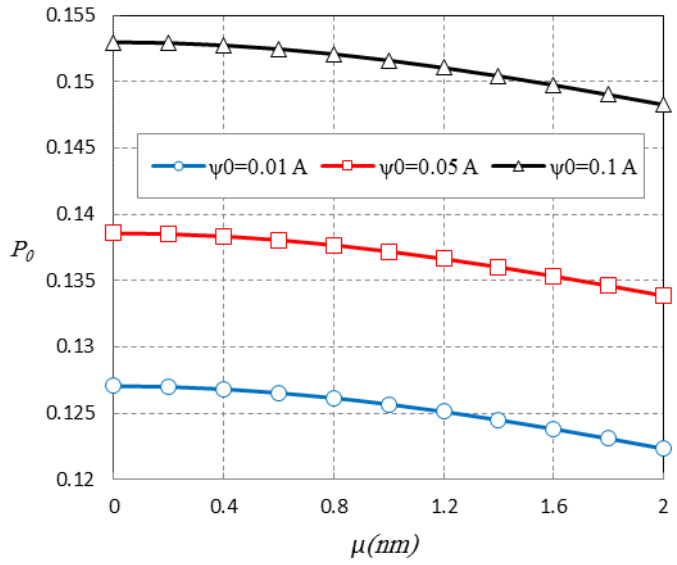

Fig. 6c. The LON parameter versus different external magnetic potential ($\mu_0 = \mu_1 = \mu$, $l=0.2h$, $\varphi_0=0.05$ V, $\Delta T=400$ K, $H_y=40\%$, $m=n=2$, $\beta=1$, A-I, SSSS)

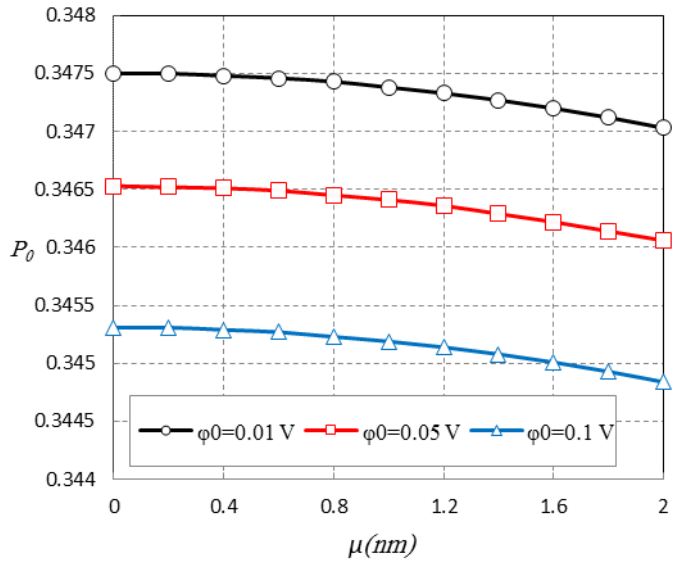

Fig. 6d. The LON parameter versus different external electric voltage ($\mu_0 = \mu_1 = \mu$, $l=0.2h$, $\psi_0=0.05$ A, $\Delta T=400$ K, $H_y=40\%$, $m=n=1$, $\beta=1$, A-II, SSSS)

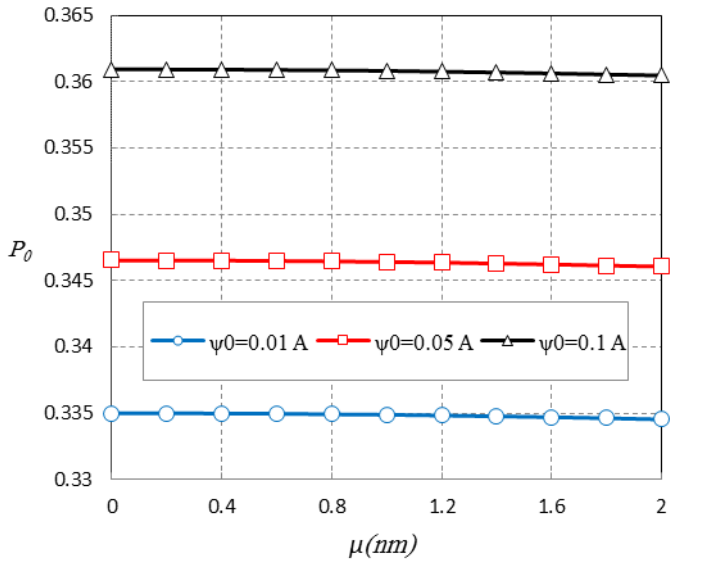

Fig. 6e. The LON parameter versus different external magnetic potential ($\mu_0 = \mu_1 = \mu$, $l=0.2h$, $\varphi_0=0.05$ V, $\Delta T=400$ K, $H_y=40\%$, $m=n=1$, $\beta=1$, A-II, SSSS)

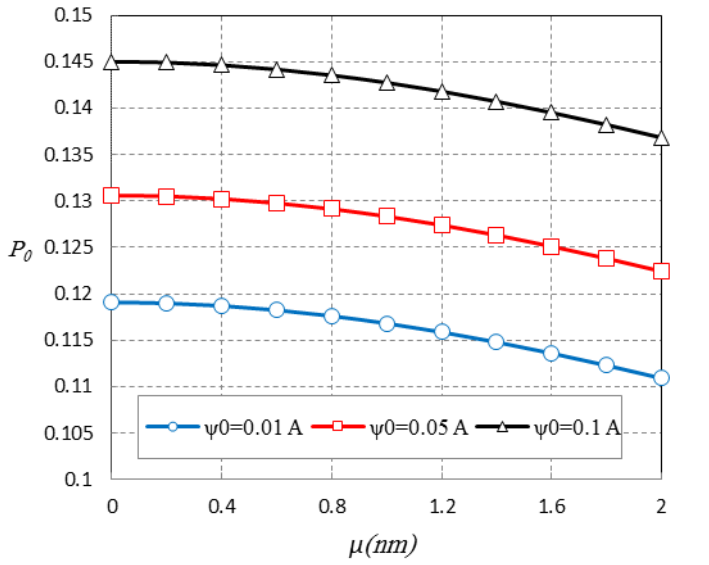

Fig. 6f. The LON parameter versus different external magnetic potential ($\mu_0 = \mu_1 = \mu$, $l=0.2h$, $\varphi_0=0.05$ V, $\Delta T=400$ K, $H_y=40\%$, $m=n=2$, $\beta=1$, A-II, SSSS)

Figs. 7a and 7b examine various boundary conditions by changing in electric and magnetic potentials under LONSG situation. The results follow the outcomes of previous figures by which it is now proved that the increase of potential field has softener influence on the plate and vice versa the grow of the magnetic field will lead to the harder plate. These results are similar for various boundary conditions and are in linear ascent or descent shapes which are because of using linear electric and magnetic potentials in the paper. One of the most complexities results in terms of these graphs could be due to linear form of the curves, which leads to very small quantities of the critical buckling loads by

increasing electric voltages. This means that in such a case for large values of the voltage, the critical buckling load will be an insignificant value and the nanoplate will buckle by a very small load.

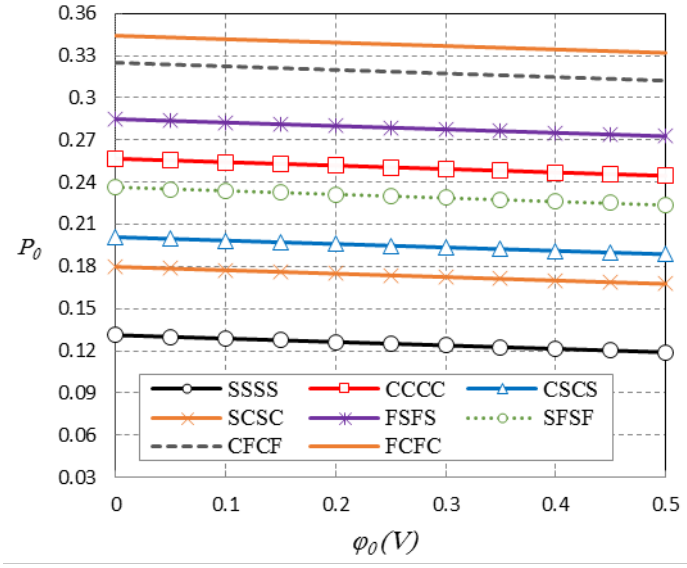

Fig. 7a. The electric voltages versus different boundary conditions ($\mu_0 = \mu_1 = 0.5$ nm, $l=0.2h$, $\psi_0=0.05$ A, $\Delta T=400$ K, $H_y=40\%$, $m=n=2$, $\beta=1$, A-II)

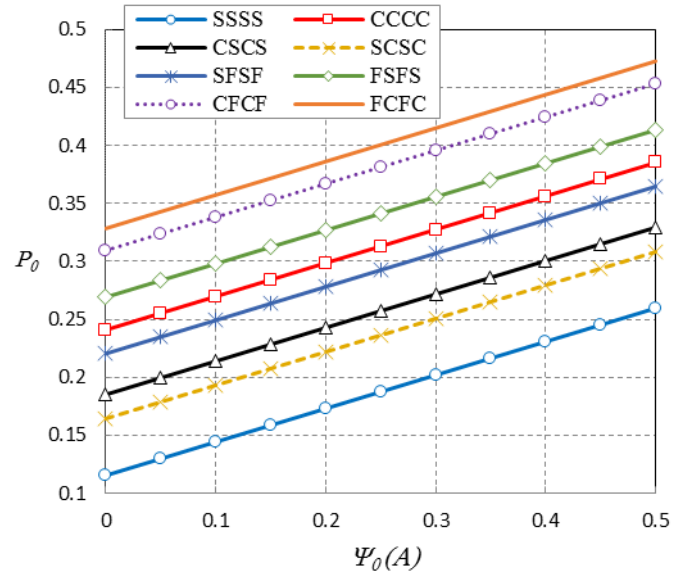

Fig. 7b. The magnetic parameter versus different boundary conditions ($\mu_0 = \mu_1 = 0.5$ nm, $l=0.2h$, $\varphi_0=0.05$ V, $\Delta T=400$ K, $H_y=40\%$, $m=n=2$, $\beta=1$, A-II)

The impact of thermal environment on the results of critical buckling loads of PMEN by considering several boundary conditions has been shown by Fig. 8. The HONSG condition is applied and the temperature influences are examined. It can be clearly seen that the temperature differential has not a great influence on the critical buckling loads, and increasing the heat decreases the critical buckling

loads slightly, which leads to monotonously reducing. In other words, the thermal environment influence is similar for all boundary conditions.

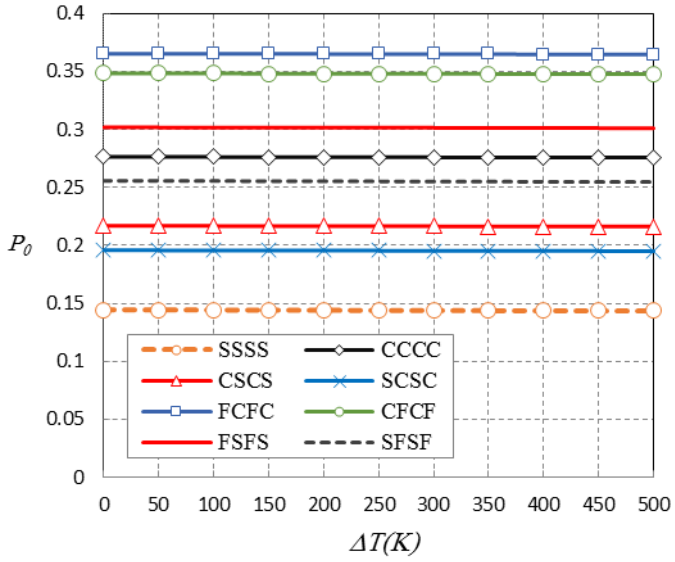

Fig. 8. Temperature changes versus different boundary conditions (μ_0= *0.2 nm,* μ_1= *0.4 nm, l=0.05h,* φ_0=*0.1 V,* ψ_0=*0.1 A,* H_y=*40%, m=n=2,* β=*1, A-II)*

The influences of moisture concentration versus different temperatures (9a) and different boundary conditions (9b) on the buckling behavior of the nanoplate are demonstrated. One of the most important observations from the figures is the major impact of hygral environment on the stability conditions of the nanoplate, that is, the stiffness of the nanoplate is markedly reduced by an increase in the moisture percentage. This is very important to notice that the impact of thermal environment is a negligible effect in comparison with that of the hygral one. In addition, it is worth noting that the slope of the results in both graphs is a linear drop. If the results of ΔT=*200 K* are doubled and the outcomes of ΔT=*400 K* are halved, the subfigure in the Fig. 9a will be turned up by which it is shown that the slopes of curves are not similar to one another. This means that the impact of moisture in lower temperatures is more considerable than that in high ones which can be an important finding.

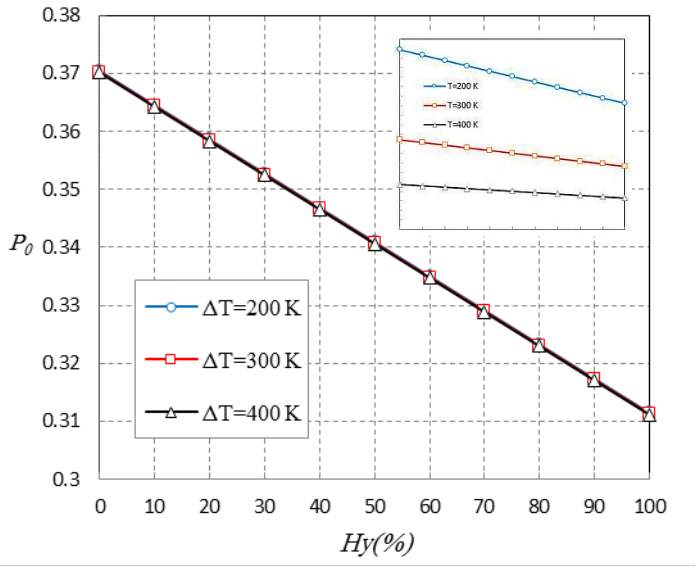

Fig. 9a. The percent of moisture versus various temperatures (μ_0=0.1 nm, μ_1=0.2 nm, l=0.02h, φ_0=0.05 V, ψ_0=0.05 A, m=n=1, β=1, A-II, SSSS)

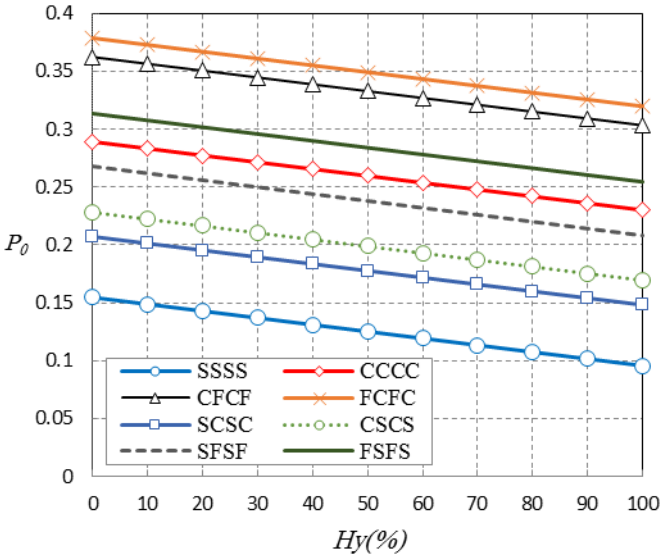

Fig. 9b. The percent of moisture versus several boundary conditions (μ_0=0.1 nm, μ_1=0.2 nm, l=0.02h, φ_0=0.05 V, ψ_0=0.05 A, ΔT=200 K, m=n=2, β=1, A-II)

To see the effects of HON and LON parameters, Fig. 10 is carried out. When the results of various cases among the three length scale parameters; μ_0, μ_1, and l, are reported, some exceptional conclusions could be harvested. Of these results are the ones between cases μ_0=0.5nm, μ_1=1nm and μ_0=1nm, μ_1=0.5nm and also cases μ_0=1nm, μ_1=2nm and μ_0=2nm, μ_1=1nm. It can be simply seen that by an increase in the SGLS factor the results of both cases are becoming closer and closer to each other. This means that greater stiffness of the nanoplate (which here results from a change in the SGLS parameter)

gives the same influences for the HON and LON factors on stability conditions. This phenomenon terminates the discussion that the HON is a tremendous operant in nanostructures analysis. And HONSG theory is strongly recommended for investigation of nanosize-dependent materials. On the other hand, Fig. 10 shows that the μ_0 decreased the critical loads more than μ_1 which leads to a point that whenever the HONSG condition is taken into consideration, the lower critical buckling loads occurred due to greater μ_0.

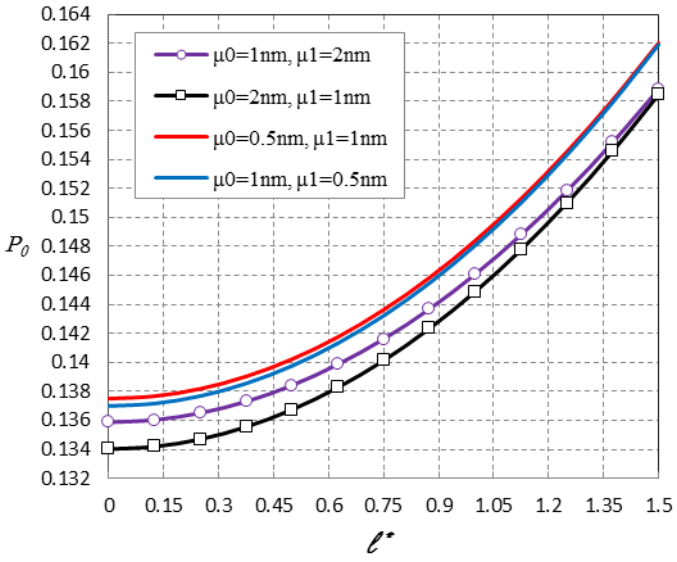

Fig. 10. The SGLS factor versus HON and LON parameters ($l^*=l/h$, $\varphi_0=0.05$ *V*, $\psi_0=0.05$ *A*, $\Delta T=400$ *K*, $H_y=40\%$, $m=n=2$, $\beta=1$, *A-I*, *SSSS*)

Fig. 11 illustrates an unpredictable impact of the SGLS parameter by which the stiffness of the nanoplate can increase or decrease by a change in SGLS. In A-I solution it was shown that the SGLS parameter has only increasing effect that in A-II some half-waves have decreasing and others have increasing influences. In fact, A-II might be more rational and reasonable than A-I because of the fact that such an assumption within which there has been supposed that in LONSG theory the length scale term in the left of the equation (LON parameter) has only softening effect and the length scale term in the right of the equation (SGLS parameter) has only hardening effect, cannot be true. Since either of the parameters has both increasing and decreasing effects regarding different conditions and situations. All in all, based on the given argument the importance of using SGLS is now clear.

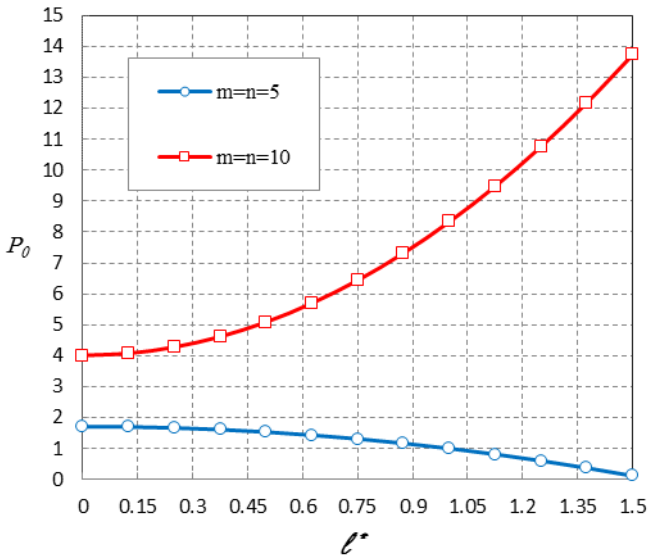

Fig. 11. The SGLS factor versus different half-waves (μ_0=0.2 nm, μ_1=0.4 nm, l^*=l/h, φ_0=0.05 V, ψ_0=0.05 A, ΔT=400 K, H_y=40%, β=1, A-II, SSSS)

5. Conclusions

This article studied the critical stability of a piezo-magnetoelectric composite ceramic nanoplate resting on an elastic matrix subjected to external in-plane mechanical forces as well as electric and magnetic potentials between the upper and bottom faces in a hygrothermal environment. To achieve this aim, a novel first-order shear deformation theory was formulated to derive the stability relations. The influences of nanoscale were considered by using the higher-order nonlocal strain gradient theory. Furthermore, the Navier's and Galerkin's solutions were employed and utilized to solve the stability equations to obtain the numerical results with taking into account several boundary conditions. The new proposed theory was first validated by comparing the obtained critical buckling loads with those from well-known available studies in the literature. Finally, influences of key parameters including low- and higher-order nonlocal, strain gradient parameters, elastic foundation coefficients, aspect ratio and environmental conditions to the nanoplate's buckling behavior were evaluated. According to the numerical results of the present study, some notable points could be expressed as follows:

* The magnetic potential has more significant influence on the critical buckling loads than the electric voltage.

* An increase in the magnetic potential led to a significant increase in the critical buckling loads and whilst an increase in the electric potential caused a decrease in the critical buckling loads.

* Thermal environment had an insignificant effect on the critical buckling loads and that was contrary to the tremendous impact of the hygral region. In particular, the stiffness of the nanoplate was significantly reduced by increasing the moisture percentage which was more noticeable in lower temperatures than in high temperatures.

* The influences of the HON and LON parameters were similar when the nanoplate's stiffness was increased. In fact, the HON parameter could be remarkably effective for large deformations (low stiffness of the plate) and therefore, the HONSG theory was strongly recommended for study of nano size-dependent materials. It should be noted that the objective of stiffness in current research is not related to high modules of elasticity and is a relative definition according to several conditions.

* The boundary conditions in which clamped edges are accompanied have been more affected by the HON parameter.

Appendix A:

$$K_{11}=\left\{\left[-D_{11}X_m''''-2\left(D_{12}+D_{66}\right)X_m''Y_n''-D_{22}Y_n''''+D_{11}\left(AX_m''''+BX_m''''Y_n''\right)+\left(D_{12}+D_{66}\right)\left(AX_m''Y_n''''+BY_n''''\right)+\right.\right.$$
$$\left.\left(D_{11}+D_{12}+D_{66}\right)\left(AX_m''''Y_n''+BX_m''Y_n''''\right)\right]-\left(\mu_1^2+l^2\right)\left[D_{11}X_m''''+2\left(D_{12}+D_{66}\right)X_m''''Y_n''+D_{22}X_m''Y_n''''+$$
$$D_{11}\left(AX_m''''''+BX_m''''Y_n''\right)+\left(D_{12}+D_{66}\right)\left(AX_m''''Y_n''''+BX_m''Y_n''''''\right)+\left(D_{11}+D_{12}+D_{66}\right)\left(AX_m''''Y_n''+BX_m''''Y_n''''\right)\Big]$$
$$-\left(\mu_1^2+l^2\right)\left[D_{11}X_m''''Y_n''+2\left(D_{12}+D_{66}\right)X_m''Y_n''''+D_{22}Y_n''''''+D_{11}\left(AX_m''''''Y_n''+BX_m''''Y_n''''\right)+\left(D_{12}+D_{66}\right)\left(AX_m''Y_n''''''+BY_n''''''\right)\right.$$
$$\left.+\left(D_{11}+D_{12}+D_{66}\right)\left(AX_m''''Y_n''''+BX_m''Y_n''''''\right)\right]+l^2\mu_0^2\left[D_{11}X_m''''''+2\left(D_{12}+D_{66}\right)X_m''''''Y_n''+D_{22}X_m''''Y_n''''+\right.$$
$$D_{11}\left(AX_m''''''+BX_m''''''Y_n''\right)+\left(D_{12}+D_{66}\right)\left(AX_m''''''Y_n''''+BX_m''''Y_n''''''\right)+\left(D_{11}+D_{12}+D_{66}\right)\left(AX_m''''''Y_n''+BX_m''''''Y_n''''\right)\Big]+$$
$$l^2\mu_0^2\left[D_{11}X_m''''Y_n''''+2\left(D_{12}+D_{66}\right)X_m''Y_n''''''+D_{22}Y_n''''''''+D_{11}\left(AX_m''''''Y_n''''+BX_m''''Y_n''''''\right)+\left(D_{12}+D_{66}\right)\times\left(AX_m''Y_n''''''''+BY_n''''''''\right)\right.$$
$$\left.+\left(D_{11}+D_{12}+D_{66}\right)\left(AX_m''''Y_n''''''+BX_m''Y_n''''''''\right)\right]+2l^2\mu_0^2\left[D_{11}X_m''''''Y_n''+2\left(D_{12}+D_{66}\right)X_m''''Y_n''''+D_{22}X_m''Y_n''''''\right.$$
$$+D_{11}\left(AX_m''''''Y_n''+BX_m''''''Y_n''''\right)+\left(D_{12}+D_{66}\right)\left(AX_m''''Y_n''''''+BX_m''Y_n''''''''\right)+\left(D_{11}+D_{12}+D_{66}\right)\left(AX_m''''''Y_n''''+BX_m''''Y_n''''''\right)\Big]+$$
$$\left(k_G\left(X_m''+Y_n''\right)-k_w\right)-\left(\mu_0^2+\mu_1^2\right)\left(k_G\left(X_m''''+2X_m''Y_n''+Y_n''''\right)-k_w\left(X_m''+Y_n''\right)\right)+\mu_0^2\mu_1^2\left(k_G\left(X_m''''''+3X_m''''Y_n''+3X_m''Y_n''''+Y_n''''''\right)\right.$$
$$\left.-k_w\left(X_m''''+2X_m''Y_n''+Y_n''''\right)\right)+N^0\times\left(A^2X_m''''''+\left(B^2+2AB\right)X_m''Y_n''''+X_m''+Y_n''+\left(2AB+A^2\right)X_m''''Y_n''+2AX_m''''+\right.$$
$$2\left(A+B\right)X_m''Y_n''+B^2Y_n''''''+2BY_n''''\Big)-N^0\left(\mu_0^2+\mu_1^2\right)\left(A^2X_m''''''+\left(B^2+2AB\right)X_m''''Y_n''''+X_m''''+X_m''Y_n''+\left(2AB+A^2\right)X_m''''Y_n''+\right.$$
$$2AX_m''''''+2\left(A+B\right)X_m''''Y_n''+B^2X_m''Y_n''''''+2BX_m''Y_n''''\Big)-N^0\left(\mu_0^2+\mu_1^2\right)\left(A^2X_m''''''Y_n''+\left(B^2+2AB\right)X_m''Y_n''''''+X_m''Y_n''+Y_n''''+\right.$$
$$\left(2AB+A^2\right)X_m''''Y_n''''+2AX_m''''Y_n''+2\left(A+B\right)X_m''Y_n''''+B^2Y_n''''''+2BY_n''''''\Big)+N^0\mu_0^2\mu_1^2\left(A^2X_m''''''+\left(B^2+2AB\right)X_m''''Y_n''''+\right.$$
$$X_m''''''+X_m''''Y_n''+\left(2AB+A^2\right)X_m''''''Y_n''+2AX_m''''''+2\left(A+B\right)X_m''''Y_n''+B^2X_m''''Y_n''''+2BX_m''''Y_n''''\Big)+N^0\mu_0^2\mu_1^2\left(A^2X_m''''''Y_n''''\right.$$
$$+\left(B^2+2AB\right)X_m''Y_n''''''+X_m''Y_n''''+Y_n''''''+\left(2AB+A^2\right)X_m''''Y_n''''+2AX_m''''Y_n''''+2\left(A+B\right)X_m''Y_n''''''+B^2Y_n''''''''+2BY_n''''''''\Big)+$$
$$2N^0\mu_0^2\mu_1^2\left(A^2X_m''''''''Y_n''+\left(B^2+2AB\right)X_m''''Y_n''''''+X_m''''Y_n''+X_m''Y_n''''+\left(2AB+A^2\right)X_m''''''Y_n''''+2AX_m''''''Y_n''++2\left(A+B\right)\times\right.$$
$$\left.X_m''''Y_n''''+B^2X_m''Y_n''''''+2BX_m''Y_n''''''\right)\Big\}$$

$$K_{12}=-\left[E_{15}\left(AX_m''''+BY_n''''+\left(A+B\right)X_m''Y_n''\right)-E_{31}\left(X_m''+Y_n''\right)\right]$$

$$K_{13}=-\left[F_{15}\left(AX_m''''+BY_n''''+\left(A+B\right)X_m''Y_n''\right)-F_{31}\left(X_m''+Y_n''\right)\right]$$

$$K_{21}=\left[E_{15}\left(AX_m''''+BY_n''''+\left(A+B\right)X_m''Y_n''\right)-E_{31}\left(X_m''+Y_n''\right)\right]$$

$$K_{22}=\left[X_{11}\left(X_m''+Y_n''\right)-X_{33}\right]$$

$$K_{23}=\left[Y_{11}\left(X_m''+Y_n''\right)-Y_{33}\right]$$

$$K_{31}=\left[F_{15}\left(AX_m''''+BY_n''''+\left(A+B\right)X_m''Y_n''\right)-F_{31}\left(X_m''+Y_n''\right)\right]$$

$$K_{32}=\left[Y_{11}\left(X_m''+Y_n''\right)-Y_{33}\right]$$

$$K_{33}=\left[Y_{22}\left(X_m''+Y_n''\right)-Y_{44}\right]$$

Appendix B:

$$R_{11} =$$

$$\int_0^{Lx}\int_0^{Ly}\left\{\begin{array}{l}
\left[-D_{11}X_m'''''Y_n-2\left(D_{12}+D_{66}\right)X_m'''Y_n''-D_{22}X_mY_n''''+D_{11}\left(AX_m'''''Y_n+BX_m'''''Y_n''\right)+\left(D_{12}+D_{66}\right)\left(AX_m'''Y_n''''+BX_mY_n'''''\right)+\right.\\
\left.\left(D_{11}+D_{12}+D_{66}\right)\left(AX_m'''''Y_n''+BX_m'''Y_n''''\right)\right]-\left(\mu_1^2+l^2\right)\left[D_{11}X_m'''''Y_n+2\left(D_{12}+D_{66}\right)X_m'''''Y_n''+D_{22}X_m'''Y_n''''+\right.\\
\left.D_{11}\left(AX_m'''''''Y_n+BX_m'''''''Y_n''\right)+\left(D_{12}+D_{66}\right)\left(AX_m'''''Y_n''''+BX_m'''Y_n'''''\right)+\left(D_{11}+D_{12}+D_{66}\right)\left(AX_m'''''''Y_n''+BX_m'''''Y_n''''\right)\right]\\
-\left(\mu_1^2+l^2\right)\left[D_{11}X_m'''''Y_n''+2\left(D_{12}+D_{66}\right)X_m'''Y_n''''+D_{22}X_mY_n'''''+D_{11}\left(AX_m'''''Y_n''+BX_m'''''Y_n''''\right)+\left(D_{12}+D_{66}\right)\times\right.\\
\left.\left(AX_m''Y_n'''''+BX_mY_n''''''\right)+\left(D_{11}+D_{12}+D_{66}\right)\left(AX_m'''''Y_n''''+BX_m'''Y_n'''''\right)\right]+l^2\mu_0^2\left[D_{11}X_m'''''Y_n+2\left(D_{12}+D_{66}\right)X_m'''''Y_n''+\right.\\
\left.D_{22}X_m'''Y_n''''+D_{11}\left(AX_m'''''''Y_n+BX_m'''''''Y_n''\right)+\left(D_{12}+D_{66}\right)\left(AX_m'''''Y_n''''+BX_m'''Y_n'''''\right)+\left(D_{11}+D_{12}+D_{66}\right)\times\right.\\
\left.\left(AX_m'''''''Y_n''+BX_m'''''Y_n''''\right)\right]+l^2\mu_0^2\left[D_{11}X_m'''''Y_n''''+2\left(D_{12}+D_{66}\right)X_m''Y_n'''''+D_{22}X_mY_n''''''+D_{11}\left(AX_m'''''Y_n''''+BX_m'''''Y_n'''''\right)\right.\\
\left.+\left(D_{12}+D_{66}\right)\times\left(AX_m''Y_n'''''+BX_mY_n'''''''\right)+\left(D_{11}+D_{12}+D_{66}\right)\left(AX_m'''Y_n''''+BX_m''Y_n''''''\right)\right]+2l^2\mu_0^2\left[D_{11}X_m'''''Y_n''+\right.\\
\left.2\left(D_{12}+D_{66}\right)X_m'''Y_n''''+D_{22}X_m''Y_n'''''+D_{11}\left(AX_m'''''Y_n''+BX_m'''''Y_n''''\right)+\left(D_{12}+D_{66}\right)\left(AX_m'''Y_n''''+BX_m''Y_n''''''\right)+\right.\\
\left.\left(D_{11}+D_{12}+D_{66}\right)\left(AX_m'''''Y_n''''+BX_m'''Y_n''''''\right)\right]+\left(k_G\left(X_m''Y_n+X_mY_n''\right)-k_w\right)-\left(\mu_0^2+\mu_1^2\right)\times\\
\left(k_G\left(X_m'''Y_n+2X_m''Y_n''+X_mY_n'''\right)-k_w\left(X_m''Y_n+X_mY_n''\right)\right)+\mu_0^2\mu_1^2\left(k_G\left(X_m'''''Y_n+3X_m'''Y_n''+3X_m''Y_n'''+X_mY_n''''\right)\right.\\
\left.-k_w\left(X_m'''Y_n+2X_m''Y_n''+X_mY_n'''\right)\right)+N^0\times\left(A^2X_m'''''Y_n+\left(B^2+2AB\right)X_m''Y_n'''+X_m''Y_n+X_mY_n''+\right.\\
\left.\left(2AB+A^2\right)X_m'''Y_n''+2AX_m'''Y_n+2\left(A+B\right)X_m''Y_n''+B^2X_mY_n''''+2BX_mY_n'''\right)-N^0\left(\mu_0^2+\mu_1^2\right)\left(A^2X_m'''''Y_n+\left(B^2+2AB\right)\right.\\
\left.X_m'''Y_n'''+X_m'''Y_n+X_m''Y_n''+\left(2AB+A^2\right)X_m''''Y_n''+2AX_m''''Y_n+2\left(A+B\right)X_m'''Y_n''+B^2X_m''Y_n''''+2BX_m''Y_n'''\right)-\\
N^0\left(\mu_0^2+\mu_1^2\right)\left(A^2X_m''''Y_n''+\left(B^2+2AB\right)X_m''Y_n''''+X_m''Y_n''+X_mY_n'''+\left(2AB+A^2\right)X_m'''Y_n'''+2AX_m'''Y_n''+2\left(A+B\right)X_m''Y_n'''\right.\\
\left.+B^2X_mY_n'''''+2BX_mY_n''''\right)+N^0\mu_0^2\mu_1^2\left(A^2X_m'''''''Y_n+\left(B^2+2AB\right)X_m''''Y_n'''+X_m''''Y_n+X_m'''Y_n''+\left(2AB+A^2\right)X_m'''''Y_n''\right.\\
\left.+2AX_m'''''Y_n+2\left(A+B\right)X_m''''Y_n''+B^2X_m'''Y_n'''''+2BX_m''Y_n''''\right)+N^0\mu_0^2\mu_1^2\left(A^2X_m''''Y_n'''+\left(B^2+2AB\right)X_m''Y_n'''''+X_m'''Y_n''''\right.\\
\left.+X_mY_n'''''+\left(2AB+A^2\right)X_m''Y_n''''+2AX_m'''Y_n'''+2\left(A+B\right)X_m''Y_n''''+B^2X_mY_n''''''+2BX_mY_n'''''\right)+2N^0\mu_0^2\mu_1^2\times\\
\left(A^2X_m'''''Y_n''+\left(B^2+2AB\right)X_m'''Y_n''''+X_m'''Y_n''+X_m''Y_n'''+\left(2AB+A^2\right)X_m''''Y_n'''+2AX_m''''Y_n''+2\left(A+B\right)\times\right.\\
\left.X_m'''Y_n'''+B^2X_m''Y_n''''+2BX_m''Y_n''''\right)
\end{array}\right\}$$

$$X_mY_n dydx$$

$$R_{12}=-\int_0^{Lx}\int_0^{Ly}\left[E_{15}\left(AX_m'''Y_n+BX_mY_n'''''+\left(A+B\right)X_m''Y_n''\right)-E_{31}\left(X_m''Y_n+X_mY_n''\right)\right]X_mY_n dydx$$

$$R_{13}=-\int_0^{Lx}\int_0^{Ly}\left[F_{15}\left(AX_m'''Y_n+BX_mY_n'''''+\left(A+B\right)X_m''Y_n''\right)-F_{31}\left(X_m''Y_n+X_mY_n''\right)\right]X_mY_n dydx$$

$$R_{21}=\int_0^{Lx}\int_0^{Ly}\left[E_{15}\left(AX_m'''Y_n+BX_mY_n'''''+\left(A+B\right)X_m''Y_n''\right)-E_{31}\left(X_m''Y_n+X_mY_n''\right)\right]X_mY_n dydx$$

$$R_{22}=\int_0^{Lx}\int_0^{Ly}\left[X_{11}\left(X_m''Y_n+X_mY_n''\right)-X_{33}X_mY_n\right]X_mY_n dydx$$

$$R_{23}=\int_0^{Lx}\int_0^{Ly}\left[Y_{11}\left(X_m''Y_n+X_mY_n''\right)-Y_{33}X_mY_n\right]X_mY_n dydx$$

$$R_{31}=\int_0^{Lx}\int_0^{Ly}\left[F_{15}\left(AX_m'''Y_n+BX_mY_n'''''+\left(A+B\right)X_m''Y_n''\right)-F_{31}\left(X_m''Y_n+X_mY_n''\right)\right]X_mY_n dydx$$

$$R_{32}=\int_0^{Lx}\int_0^{Ly}\left[Y_{11}\left(X_m''Y_n+X_mY_n''\right)-Y_{33}X_mY_n\right]X_mY_n dydx$$

$$R_{33}=\int_0^{Lx}\int_0^{Ly}\left[Y_{22}\left(X_m''Y_n+X_mY_n''\right)-Y_{44}X_mY_n\right]X_mY_n dydx$$

References

[1] J. V. Suchetelene, Product Properties: A New Application of Composite Materials, Philips research reports, 27 (1972) 28-37.

[2] R. Ramesh, N. A. Spaldin, Multiferroics: progress and prospects in thin films, Nature Materials, 6 (2007) 6-21.

[3] N. A. Hill, Why are there so few magnetic ferroelectrics?, The Journal of Physical Chemistry B, 104 (2000) 6694-6709.

[4] J. P. Zhou, H. C. He, Z. Shi, C. W. Nan, Magnetoelectric CoFeO /Pb (ZrTi) O double-layer thin film prepared by pulsed-laser deposition, Applied Physics Letters, 01311 (2006) 1-3.

[5] R. S. Devan, S. B. Deshpande, and B. K. Chougule, Ferroelectric and ferromagnetic properties of (x) BaTiO / (1-x) NiCo CuFeO composite, Journal of Physics D: Applied Physics, 40 (2007) 1864-1868.

[6] M. Avellaneda, G. Harshe, Magnetoelectric effect in piezoelectric/magnetostrictive multilayer (2-2) composites, Journal of Intelligent Material Systems and Structures, 5 (1994) 501-513.

[7] G. Srinivasan, E. T. Rasmussen, J. Gallegos and R. Srinivasan., Magnetoelectric bilayer and multilayer structures of magnetostrictive and piezoelectric oxides Physical Review B, 64 (2001) 1-6.

[8] S. Lopatina, I. Lopatina and I. Lisnevskaya S., Magnetoelectric PZT/ferrite composite material, Ferroelectrics, 162 (1994) 63-68.

[9] C-W. Nan, Magnetoelectric effect in composites of piezoelectric and piezomagnetic phases, Physical Review B, 50 (1994) 6082-6088.

[10] Lutgard C. De Jonghie, Mohamed N. Rahman, Sintering of Ceramics, handbook of advanced ceramics, 2003.

[11] L. L. Ke, Y. S. Wang, Z. D. Wang, Nonlinear vibration of the piezoelectric nanobeams based on the nonlocal theory, Composite Structures, 94 (2012) 2038–2047.

[12] C. Liu, L. L. Ke, Y. S. Wang, J. Yang, Kitipornchai S. Buckling and post-buckling of size-dependent piezoelectric Timoshenko nanobeams subject to thermo-electro-mechanical loadings, International Journal of Structural Stability and Dynamics, 14 (2014) 1350067.

[13] L. Y. Jiang, Z. Yan, Vibration and buckling analysis of a piezoelectric nanoplate considering surface effects and in-plane constraints, Proceedings of the Royal Society of London. Series A, 468 (2012) 3458-3475.

[14] X. Q. Fang, Ch. S. Zhu, Size-dependent nonlinear vibration of nonhomogeneous shell embedded with a piezoelectric layer based on surface/interface theory, Composite Structures, 160 (2017) 1191–1197.

[15] Ch. S. Zhu, X. Q. Fang, J. X. Liu, H. Y. Li, Surface energy effect on nonlinear free vibration behavior of orthotropic piezoelectric cylindrical nano-shells, European Journal of Mechanics / A Solids, 66 (2017) 423-432.

[16] A. Jamalpoor, A. Ahmadi-Savadkoohi, M. Hossein, Sh. Hosseini-Hashemi, Free vibration and biaxial buckling analysis of double magneto-electro-elastic nanoplate-systems coupled by a Visco-Pasternak medium via nonlocal elasticity theory, European Journal of Mechanics / A Solids, 63 (2017) 84-98.

[17] R. Gholami, R. Ansari, A unified nonlocal nonlinear higher-order shear deformable plate model for postbuckling analysis of piezoelectric-piezomagnetic rectangular nanoplates with various edge supports, Composite Structures, 166 (2017) 202–218.

[18] M. Arefi, A. M. Zenkour, Size-dependent free vibration and dynamic analyses of piezo-electro-magnetic sandwich nanoplates resting on viscoelastic foundation, Physica B: Physics of Condensed Matter, 521 (2017) 188-197.

[19] S. Sahmani, M. M. Aghdam, Nonlocal strain gradient shell model for axial buckling and postbuckling analysis of magneto-electro-elastic composite nanoshells, Composites Part B: Engineering, 132 (2018) 258-274.

[20] R. Ansari, M. Faraji Oskouie, R. Gholami, F. Sadeghi, Thermo-electro-mechanical vibration of postbuckled piezoelectric Timoshenko nanobeams based on the nonlocal elasticity theory, Composites Part B: Engineering, 89 (2016) 316-327.

[21] R. Ansari, R. Gholami, H. Rouhi, size-dependent nonlinear forced vibration analysis of magneto-electro-thermo-elastic Timoshenko nanobeams based upon the Nonlocal elasticity theory, Composite Structures, Composite Structures, 126 (2015) 216-226.

[22] R. Ansari, E. Hasrati, R. Gholami, F. Sadeghi, Nonlinear analysis of forced vibration of nonlocal third-order shear deformable beam model of magneto-electro-thermo elastic nanobeams, Composites Part B: Engineering, 83 (2015) 226-241.

[23] R. Ansari, R. Gholami, nonlocal nonlinear first-order shear deformable beam model for post-buckling analysis of magneto-electro-thermo-elastic nanobeams, Scientia Iranica, 23 (2016) 3099-3114.

[24] R. Gholami, R. Ansari, Y. Gholami, Size-dependent bending, buckling and vibration of higher-order shear deformable magneto-electro-thermo-elastic rectangular nanoplates, Materials Research Express, 4 (2017) 065702.

[25] M. Malikan, Temperature influences on shear stability of a nanosize plate with piezoelectricity effect, Multidiscipline modeling in materials and structures, 14 (2018) 125-142.

[26] R. Ansari, R. Gholami, size-dependent buckling and postbuckling analyses of first-order shear deformable magneto-electro-thermo elastic nanoplates based on the nonlocal elasticity theory, International Journal of Structural Stability and Dynamics, 17 (2017) 1750014.

[27] R. Ansari, R. Gholami, Nonlocal free vibration in the pre- and post-buckled states of magneto-electro-thermo elastic rectangular nanoplates with various edge conditions, Smart Materials and Structures, 25 (2016) 095033.

[28] R. Ansari, R. Gholami, size-dependent nonlinear vibrations of first-order shear deformable magneto-electro-thermo elastic nanoplates based on the nonlocal elasticity theory, International Journal of Applied Mechanics, 8 (2016) 1650053.

[29] Q. Deng, Size-dependent flexoelectric response of a truncated cone and the consequent ramifications for the experimental measurement of flexoelectric properties, Journal of Applied Mechanics, 84 (2017) 101007.

[30] F. Ebrahimi, M. R. Barati, Free vibration analysis of couple stress rotating nanobeams with surface effect under in-plane axial magnetic field, Journal of vibration and control, (2017), https://doi.org/10.1177/1077546317744719.

[31] Q. Ma, D. R. Clarke, Size Dependent Hardness in Silver Single Crystals, Journal of Materials Research, 10 (1995) 853-863.

[32] W. J. Poole, M. F. Ashby, N. A. Fleck, Micro-Hardness of Annealed and Work-Hardened Copper Polycrystals, Scripta Materialia, 34 (1996) 559-564.

[33] Y. Y. Lim, Y. Y. Chaudhri, The Effect of the Indenter Load on the Nanohardness of Ductile Metals: An Experimental Study of Polycrystalline Work-Hardened and Annealed Oxygen-Free Copper, Philosophical Magazine A, 79 (1999) 2979-3000.

[34] H. Askes, E. C. Aifantis, Gradient elasticity and flexural wave dispersion in carbon nanotubes, Physical Review B, 80 (2009) 195412.

[35] A. Nateghi, M. Salamat-talab, Thermal effect on size dependent behavior of functionally graded microbeams based on modified couple stress theory, Composite Structures, 96 (2013) 97–110.

[36] D. C. C. Lam, F. Yang, A. C. M. Chong, J. Wang, P. Tong, Experiments and theory in strain gradient elasticity, Journal of the Mechanics and Physics of Solids, 51 (2003) 1477–508.

[37] L-L. Ke, Y-S. Wang, Size effect on dynamic stability of functionally graded microbeams based on a modified couple stress theory, Composite Structures, 93 (2011) 342–50.

[38] H. M. Ma, X. L. Gao, J. N. Reddy, A microstructure-dependent Timoshenko beam model based on a modified couple stress theory, Journal of the Mechanics and Physics of Solids, 56 (2008) 3379–91.

[39] A. C. Eringen, On differential equations of nonlocal elasticity and solutions of screw dislocation and surface waves, Journal of Applied Physics, 54 (1983) 4703–4710.

[40] A. C. Eringen, Linear theory of non-local elasticity and dispersion of plane waves, International Journal of Engineering Sciences, 10 (1972) 425-435.

[41] S. Narendar, S. Gopalakrishnan, Scale effects on buckling analysis of orthotropic nanoplates based on nonlocal two-variable refined plate theory, Acta Mechanica, 223 (2012) 395–413.

[42] W. H. Duan, C. M. Wang, Exact solutions for axisymmetric bending of micro/nanoscale circular plates based on nonlocal plate theory, Nanotechnology, 18 (2007) 385704.

[43] W. H. Duan, C. M. Wang, and Y. Y. Zhang, Calibration of nonlocal scaling effect parameter for free vibration of carbon nanotubes by molecular dynamics, Journal of Applied Physics, 101, 024305 (2007); doi: 10.1063/1.2423140.

[44] D. Shahsavari, B. Karami, S. Mansouri, Shear buckling of single layer graphene sheets in hygrothermal environment resting on elastic foundation based on different nonlocal strain gradient theories, European Journal of Mechanics / A Solids, 67 (2018) 200-214.

[45] M. Malikan, M. Jabbarzadeh, Sh. Dastjerdi, Non-linear Static stability of bi-layer carbon nanosheets resting on an elastic matrix under various types of in-plane shearing loads in thermo-elasticity using nonlocal continuum, Microsystem Technologies, 23 (2017) 2973-2991.

[46] F. Ebrahimi, M. R. Barati, (2018), vibration analysis of biaxially compressed double-layered graphene sheets based on nonlocal strain gradient theory, Mechanics of Advanced Materials and Structures, doi: 10.1080/15376494.2018.1430267.

[47] M. Malikan, Electro-mechanical shear buckling of piezoelectric nanoplate using modified couple stress theory based on simplified first order shear deformation theory, Applied Mathematical Modelling, 48 (2017) 196–207.

[48] M. Malikan, Analytical predictions for the buckling of a nanoplate subjected to nonuniform compression based on the four-variable plate theory, Journal of Applied and Computational Mechanics, 3 (2017) 218–228.

[49] M. Malikan, Buckling analysis of a micro composite plate with nano coating based on the modified couple stress theory, Journal of Applied and Computational Mechanics, 4 (2018) 1–15.

[50] R. P. Shimpi, Refined Plate Theory and Its Variants, AIAA JOURNAL, 40 (2002).

[51] C. Liu, L. L. Ke, J. Yang, S. Kitipornchai, Y.S. Wang, Buckling and post-buckling analysis of size-dependent piezoelectric nanoplates, Theoretical & Applied Mechanics Letters, 6 (2016) 253-267.

[52] D. P. Zhang , Y. J. Lei , Z. B. Shen, Thermo-electro-mechanical vibration analysis of piezoelectric nanoplates resting on viscoelastic foundation with various boundary conditions, International Journal of Mechanical Sciences, 131–132 (2017) 1001-1015.

[53] C. W. Lim, G. Zhang, J. N. Reddy, A Higher-order nonlocal elasticity and strain gradient theory and Its Applications in wave propagation, Journal of the Mechanics and Physics of Solids, 78 (2015) 298-313.

[54] M. S. Nematollahi, H. Mohammadi, M. A. Nematollahi, Thermal vibration analysis of nanoplates based on the higher-order nonlocal strain gradient theory by an analytical approach, Superlattices and Microstructures, 111 (2017) 944-959.

[55] A. Farajpour, M. R. Haeri Yazdi, A. Rastgoo, M. Mohammadi, A higher-order nonlocal strain gradient plate model for buckling of orthotropic nanoplates in thermal environment, Acta Mechanica, 227 (2016) 1849–1867.

[56] N. Fleck, J. Hutchinson, A reformulation of strain gradient plasticity, Journal of the Mechanics and Physics of Solids, 49 (2001) 2245–2271.

[57] Long Zhang, Ph.D, Binglei Wang, Shenjie Zhou, and Yiguo Xue, Modeling the Size-Dependent Nanostructures: Incorporating the Bulk and Surface Effects, Journal of Nanomechanics and Micromechanics, (2017), https://doi.org/10.1061/(ASCE)NM.2153-5477.0000117.

[58] Yarong Zhou, Xu Yang, Dongmei Pan, Binglei Wang, Improved incorporation of strain gradient elasticity in the flexoelectricity based energy harvesting from nanobeams, Physica E: Low-dimensional Systems and Nanostructures, 98 (2018) 148–158.

[59] A. C. Eringen, Nonlocal continuum field theories, Springer, New York, (2002).

[60] Chih-Ping Wu, Wei-Chen Li, Asymptotic nonlocal elasticity theory for the buckling analysis of embedded single-layered nanoplates/graphene sheets under biaxial compression, Physica E: Low-dimensional Systems and Nanostructures, 89 (2017) 160-169.

[61] R. D. Mindlin, Second gradient of train and surface-tension in linear elasticity, International Journal of Solids and Strucutres, 1 (1965) 417-438.

[62] R. D. Mindlin, N. N. Eshel, On first strain-gradient theories in linear elasticity, International Journal of Solids and Strucutres, 4 (1968) 109-124.

[63] Junhong Guo, Jiangyi Chen, Ernian Pan, Free vibration of three-dimensional anisotropic layered composite nanoplates based on modified couple-stress theory, Physica E: Low-dimensional Systems and Nanostructures, 87 (2017) 98-106.

[64] R. D. Mindlin, Micro-structure in linear elasticity, Archive for Rational Mechanics and Analysis, 16 (1964) 51-78.

[65] R. A. Toupin, Elastic materials with couple stresses, Archive for Rational Mechanics and Analysis, 11 (1962) 385-414.

[66] R. A. Toupin, Theories of elasticity with couple-stress, Archive for Rational Mechanics and Analysis, 17 (1964) 85-112.

[67] R. D. Mindlin, H. F. Tiersten, Effects of couple-stresses in linear elasticity, Archive for Rational Mechanics and Analysis, 11 (1962) 415-448.

[68] D. Rogula, Nonlocal theory of material media, Springer, New York, (2002) 376 pages.

[69] H. Askes, E. C. Aifantis, Gradient elasticity in statics and dynamics: An overview of formulations, length scale identification procedures, finite element implementations and new results, International Journal of Solid and Structures, 48 (2011) 1962-1990.

[70] R. Ansari, J. Torabi, A. Norouzzadeh, Bending analysis of embedded nanoplates based on the integral formulation of Eringen′s nonlocal theory using the finite element method, Physica B: Condensed Matter, 534 (2018) 90-97.

[71] V. E. Tarasov, General lattice model of gradient elasticity, Modern Physics Letters B., 28 (2014) 1450054.

[72] M. Rubin, P. Rosenau, O. Gottlieb, Continuum model of dispersion caused by an inherent material characteristic length, Journal of Applied physics, 77 (1995) 4054-4063.

[73] A. V. Metrikine, H. Askes, One-dimensional dynamically consistent gradient elasticity models derived from a discrete microstructures. Part 1: Generic formulation, European journal of mechanics – A/Solids., 21 (2002) 555-572.

[74] B. Karami, D. Shahsavari, L. Li, Hygrothermal wave propagation in viscoelastic graphene under in-plane magnetic field based on nonlocal strain gradient theory, Physica E: Low-dimensional Systems and Nanostructures, 97 (2018) 317-327.

[75] R. Ansari, T. Pourashraf, R. Gholami, A. Shahabodini, Analytical solution for nonlinear postbuckling of functionally graded carbon nanotube-reinforced composite shells with piezoelectric layers, Composites Part B: Engineering, 90 (2016) 267-277.

[76] Na-Ho Kim, Introduction to finite element methods, Wiley 2008.

[77] M. Malikan, M. N. Sadraee Far, Differential quadrature method for dynamic buckling of graphene sheet coupled by a viscoelastic medium using neperian frequency based on nonlocal elasticity theory, Journal of Applied and Computational Mechanics,

DOI: 10.22055/JACM.2017.22661.1138, (2018).

[78] A. Gawandi, J. M. Whitney, Natural boundary conditions in the bending of anisotropic laminated plates, Composite Structures, 82 (2008) 201-208.

[79] M. E. Golmakani, J. Rezatalab, Nonuniform biaxial buckling of orthotropic Nano plates embedded in an elastic medium based on nonlocal Mindlin plate theory, Composite Structures, 119 (2015) 238-250.

[80] M. E. Golmakani, M. N. Sadraee Far, Buckling analysis of biaxially compressed double-layered graphene sheets with various boundary conditions based on nonlocal elasticity theory, Microsystem Technologies, 23 (2017) 2145-2161.

[81] R. Ansari, S. Sahmani, Prediction of biaxial buckling behavior of single-layered graphene sheets based on nonlocal plate models and molecular dynamics simulations, Applied Mathematical Modelling, 37 (2013) 7338–51.

[82] L. L. Ke, Y. S. Wang, J. Yang, S. Kitipornchai, Free vibration of size-dependent magneto-electro-elastic nanoplates based on the nonlocal theory, Acta Mechanica Sinica, 30 (2014) 516–25.

[83] A. Farajpour, A. Rastgoo, M.R. Farajpour, Nonlinear buckling analysis of magneto-electro-elastic CNT-MT hybrid nanoshells based on the nonlocal continuum mechanics, Composite Structures, 180 (2017) 179-191.

[84] A. M. Zenkour, M. Sobhy, Nonlocal piezo-hygrothermal analysis for vibration characteristics of a piezoelectric Kelvin-Voigt viscoelastic nanoplate embedded in a viscoelastic medium, Acta Mechanica, 229 (2018) 3–19.

[85] R. Gholami, R. Ansari, Size-dependent geometrically nonlinear free vibration of first-order shear deformable piezoelectric-piezomagnetic nanobeams using the nonlocal theory, Advances in Applied Mathematics and Mechanics, 10 (2018) 184-208.